Biomedicine & Pharmacotherapy 188 (2025) 118162

Contents lists available at ScienceDirect

Biomedicine & Pharmacotherapy

journal homepage: www.elsevier.com/locate/biopha

Stem cell-mediated bone regeneration of marine-derived fibrinolytic compound (FGFC-1) loaded carboxymethyl chitosan hydrogels

Lakshmi Jeevithan [a,b], Wang Shuyue [a], Sabu Thomas [c], Jose Eduardo Mate Sanchez de Val [b], Wenhui Wu [a,*], Jeevithan Elango [a,b,**]

[a] Department of Marine Bio-Pharmacology, College of Food Science and Technology, Shanghai Ocean University, Shanghai 201306, China
[b] Department of Biomaterials Engineering, Faculty of Health Sciences, UCAM-Universidad Católica San Antonio de Murcia, Campus de los Jerónimos, 135, Guadalupe, Murcia 30107, Spain
[c] School of Chemical Sciences, Mahatma Gandhi University, Kottayam, Kerala 686560, India

ARTICLE INFO

Keywords:
Hydrogel
Carboxymethyl chitosan
Marine fungi
Osteogenesis
Stem cell regeneration

ABSTRACT

Carboxymethyl chitosan (CMC)-based hydrogels (HG) have gained significant attention for therapeutic applications due to their biomimetic properties and biocompatibility. This study explores, for the first time, the regenerative and osteogenic potential of CMC-HG incorporated with a marine fungi-derived fibrinolytic compound, FGFC-1. The inclusion of FGFC-1 did not significantly alter the crucial characteristics of the HGs, including secondary structure, thermal stability, protein adhesion, and in vitro degradation. However, incorporation of FGFC1 increased the swelling capacity (from 132.88 % to 157.11 %) and decreased the mineral adhesion (0.416 at 0.1 mg/ml) and porosity (from 72.95 % to 54.29 %). In general, the bacterial adhesion was decreased by 44.3 % in HG than control., Optimal culture conditions for mesenchymal stem cells (MSCs) were achieved with 2 % CMC and FGFC-1 concentrations of 0.01–1 mg/ml (Supplementary Fig. S2), supporting significant MSC growth. SEM image proved more interconnected dense fibrillar clustered morphology of MSCs on HGs than 2D. FGFC-1 accelerated osteogenic differentiation of MSCs by increasing mRNA expression levels of Runx2 (4.98), collagen-1 alpha-1 (3.4), osteocalcin (3.62), and ALP (4.20), which was further validated through enhanced staining for alizarin red, von Kossa, and alkaline phosphatase, as well as immunostaining for osteocollagen and osteocalcin in differentiated MSCs within the hydrogels. Notably, FGFC-1 significantly induced osteogenic differentiation along with supplements. These findings highlight FGFC-1-loaded CMC hydrogels as a promising strategy for stem cell-mediated bone regeneration in biomedical applications.

1. Introduction

Hydrogels are innovative materials known for their exceptional water-retaining capabilities and structural integrity. These hydrophilic, three-dimensional polymer networks have become pivotal in the biomedical field due to their versatility and biocompatibility [1,2]. Hydrogels can absorb and retain significant amounts of water, making them ideal for various medical applications [3]. In drug delivery systems, hydrogels provide controlled and sustained release of therapeutic agents, enhancing treatment efficacy and patient compliance[4]. Their ability to mimic the natural extracellular matrix makes them invaluable in tissue engineering, where they support cell growth and tissue regeneration. Wound healing benefits from hydrogels' moisture-retentive properties, which create an optimal environment for tissue repair and reduce infection risks [5]. Additionally, hydrogels are employed in biosensors, where their responsive nature to environmental stimuli allows for accurate and real-time monitoring of biological signals. The adaptability of hydrogels extends to their mechanical properties, which can be tailored to meet specific biomedical needs. This tunability, combined with their biocompatibility and biodegradability, positions hydrogels as essential components in advancing healthcare technologies [6]. As research progresses, the potential applications of hydrogels in the biomedical field continue to expand, promising innovative solutions for complex medical challenges.

* Corresponding author.
** Correspondence to: Department of Biomaterials Engineering, Faculty of Health Sciences, UCAM-Universidad Católica San Antonio de Murcia, Campus de los Jerónimos 135, Guadalupe, 30107 Murcia, Spain.
E-mail addresses: whwu@shou.edu.cn (W. Wu), jelango@ucam.edu (J. Elango).

https://doi.org/10.1016/j.biopha.2025.118162
Received 26 March 2025; Received in revised form 30 April 2025; Accepted 9 May 2025
Available online 14 May 2025

Among the wide range of biopolymers used in hydrogel fabrication, carboxymethyl chitosan (CMC) is a versatile and widely researched material, known for its impressive properties and diverse applications [7]. CMC is a derivative of chitosan, a biopolymer obtained from chitin, which is primarily sourced from the shells of crustaceans. CMC is characterized by the introduction of carboxymethyl groups into the chitosan structure, enhancing its solubility in water and expanding its range of applications[8]. This modification not only improves the functional properties of chitosan but also imparts unique characteristics that make CMC a valuable material in various fields, including pharmaceuticals, agriculture, and food technology [7]. The biocompatibility, biodegradability, and non-toxicity of CMC further contribute to its appeal, positioning it as a promising candidate for innovative applications in drug delivery systems, wound healing, and as a food preservative[9, 10]. Hence, the hydrogel fabrication from CMC could be an ideal concept due to their tuneable properties through various chemical modifications, allowing for tailored performance in specific applications in wound healing, drug release, and as scaffolds for tissue regeneration.

Similarly, marine-derived secondary metabolites are a fascinating and diverse group of natural compounds produced by marine organisms such as bacteria, fungi, sponges, algae, and corals [11]. These metabolites are not essential for the basic metabolic processes of the organisms but play crucial roles in their survival, often serving as defense mechanisms against environmental stressors. The unique and often extreme conditions of marine environments, such as high pressure, low temperature, and limited light, drive the evolution of these compounds, resulting in a remarkable chemical diversity that is rarely found in terrestrial organisms [12]. One of the most exciting aspects of marine-derived secondary metabolites is their potential for pharmaceutical applications. Many of these compounds exhibit potent bioactivities, including anticancer [13], antimicrobial [14,15], antioxidant [15,16], antiviral [16], and anti-inflammatory [17].

For instance, compounds like bryostatin, derived from marine bryozoans, have shown promise in cancer therapy[18], while others like ziconotide, derived from cone snail venom, are used as powerful painkillers[19]. The structural complexity and novel mechanisms of action of these metabolites make them valuable leads for drug discovery and development. Research into marine-derived secondary metabolites is still in its early stages, but it holds great promise for the future. By understanding and utilizing the chemical diversity of marine secondary metabolites, we can develop new and innovative treatments for a wide range of diseases, highlighting the importance of preserving marine biodiversity and ecosystems. Hence, marine-derived secondary metabolites have been gaining significant attention recently in regenerative engineering due to their unique bioactive properties. For instance, our recent studies explored the isolation, chemical characteristics, and biological responses (fibrinolytic and anticancer) of marine Fungi Fibrinolytic compound 1 (FGFC-1)[20–22]. Despite the growing interest in marine-derived secondary metabolites, their potential in regenerative medicine remains largely unexplored. This study pioneers the incorporation of FGFC-1 into CMC hydrogels, marking the first investigation of its biological effects in bone tissue engineering. By integrating FGFC-1 within a hydrogel matrix, this work aims to enhance osteogenic differentiation, demonstrating a novel biomaterial-based strategy for targeted regenerative applications Scheme 1.

2. Methods and materials

2.1. Extraction of FGFC-1 from Stachybotrys longispora. FG216

FGFC-1 (≥98 % purity) was isolated and purified from the methanol extracts of *Stachybotrys longispora*. FG216, as previously outlined in studies by Wang et al. [23] and Guo et al. [20]. In brief, the medium of FG216 fermented samples underwent centrifugation to collect Marine microorganism precipitate (200 g), which was then dissolved in methanol to a total volume of 2 L. Following ultrasonic extraction, the methanol-immersed sample was concentrated under vacuum at temperatures ranging from 40 to 60°C. The sample was dissolved in 60 % saturation NaCl solution and adjusted to pH 3.0 using 6 N HCl. Subsequently, the acid solution underwent triple extraction with ethyl acetate. The ethyl acetate layer was then subjected to triple extraction with a saturated NaCl solution. Finally, the acid solution layer was concentrated under vacuum and dissolved to yield the crude extract. This extract was then subjected to preparative High Performance Liquid Chromatography (HPLC) using an Inertsil PREP-ODS column (22.5 × 250 mm) at 40°C, with a gradient elution of acetonitrile and 0.1 % trifluoroacetic acid at a flow rate of 10 ml/min. Following extraction with ethyl acetate, the purified compounds were evaporated to remove acetonitrile and trifluoroacetic acid from the fractions containing the fibrinolytic products. FGFC-1 was dissolved in DMSO to create a stock solution, which could be easily diluted to various concentrations with cell culture medium prior to use.

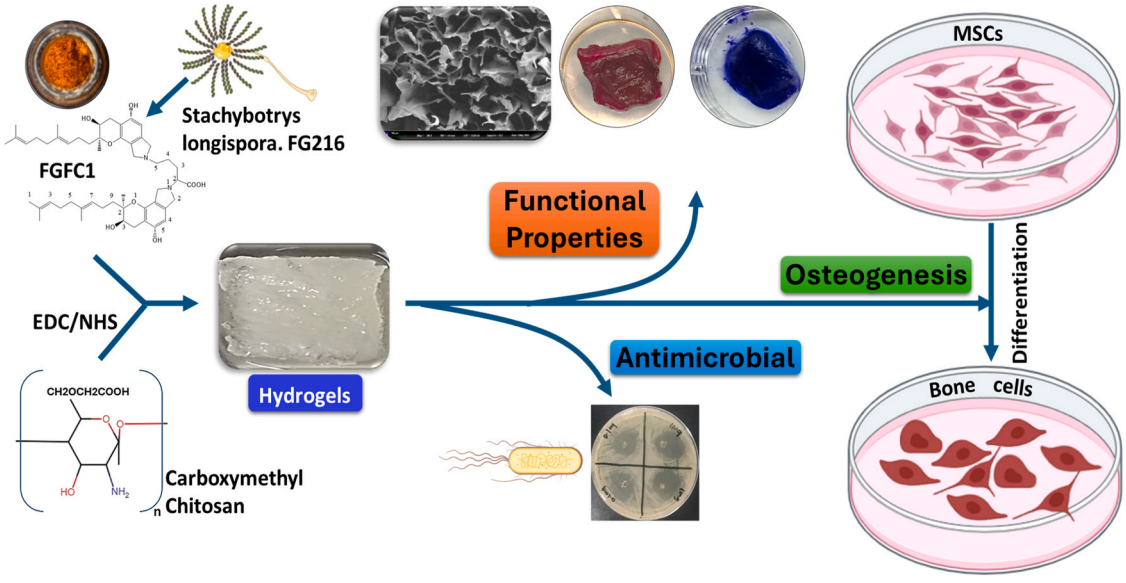

Scheme 1. Overall schematic representation of the study design.

2.2. Fabrication of CMC-FGFC-1 hydrogels

In order to optimize the raw materials for hydrogel fabrication, different concentrations (1,2 and 3 %) of carboxymethyl chitosan (Sigma- Aldrich, Shanghai, China, CAS Number:83512–85–0), (Carboxymethylation >/=80 %, Molecular weight: 543.519 g/mol, Molecular formula: (C8H13NO6)n(C8H13NO5)m, viscosity: 200–300 cps) (Molecular structure provided in Supplementary Fig.S1) and FGFC-1 (1 ng, 10 ng, 100 ng, 1 ug, 10 ug, 100 ug and 1 mg/ml) were treated with bone marrow mesenchymal stem cells and measured cell viability using CCK-8 method as described below.

Based on the results (supplementary Fig S2), 2 % CMC and 0.01, 0.1 and 1 mg/ml FGFC-1 were chosen for hydrogel fabrication. Briefly, the 0.2 g CMC (2 %) was completely dissolved in distilled water and crosslinked with EDC/NHS (0.011 g/20.5 µl, respectively) at 37 °C for 12–18 hours. This was considered as control (C) hydrogel. For FGFC-1 group, different concentrations of FGFC-1 (0.01, 0.1 and 1 mg/ml) were mixed with control hydrogel and labeled as HG-0.01, HG-0.1 and HG-1, respectively (Fig. 1).

2.3. Characterization

2.3.1. Swelling and porosity

To investigate the characteristics of hydrogel, the swelling capacity and porosity of hydrogel were tested using freeze-dried samples by following earlier methods [24]. Briefly, the dry weight of freeze-dried samples (Wd) was measured before incubation in the medium. To assess swelling capacity and porosity, freeze-dried samples were incubated in distilled water for 5 hours and in 99.9 % ethanol for 1 hour [24, 25]. Swelling capacity was determined by measuring the difference in water absorption before and after incubation, while porosity was evaluated based on the amount of ethanol penetrating the hydrogel pores after incubation. In both cases, the final weights (Ww) were measured following the removal of excess water or ethanol from the sample surfaces using filter papers. The swelling rate (SR) and porosity of samples were measured by using the below formulas.

$$SR = (Ww\text{-}Wd/Wd)x\ 100,\ Porosity\ (\%) = (Ww\text{-}Wd)/\ \rho V$$

Where, Ww- final weights after incubation, Wd- dry weight of freeze-dried samples before incubation, ρ is a constant representing the density of ethanol and V is the volume.

2.3.2. In vitro biodegradation rate

The invitro biodegradation of freeze-dried samples was determined by following earlier methods reported[26,27]. Briefly, the samples were incubated in PBS (pH 7.4) with 8 × 104 U/ml lysozyme at 37 °C. Degradation was evaluated by measuring weight loss at various time intervals (1, 3, 5, 7, 14, and 21 days). The samples were weighed at each time point, and the degradation ratio was then calculated.

$$D = (W_0\text{-}W_t)/W_0 x\ 100\%$$

where W_0 – dry (initial) weight of freeze-dried samplesW_t - the sample weight after incubation in a lysozyme solution for *t* days.

2.3.3. Fourier-transform infrared spectroscopy (FTIR)

The determination of secondary structural changes in hydrogels induced by CMC and various concentrations of FGFC-1 during the manufacturing process was carried out through the collection of FTIR spectra using a Fourier transform infrared spectrometer (L1050050 Spotlight 400, PerkinElmer Co., Hopkinton, MA, USA). An initial air background was utilized for the FTIR spectra acquisition. The instrument plate was loaded with 2 mg of samples, and absorption spectra were captured within the range of 400–4000 cm−1 in absorption mode at 4 cm−1 intervals for 32 scans using an attenuated total reflection (ATR) accessory. Any interferences from H2O and CO2 were effectively removed during the procedure. The secondary structure analysis of the samples was conducted using PeakFit Version 4 software (SeaSolve software Inc., Framingham, MA, USA).

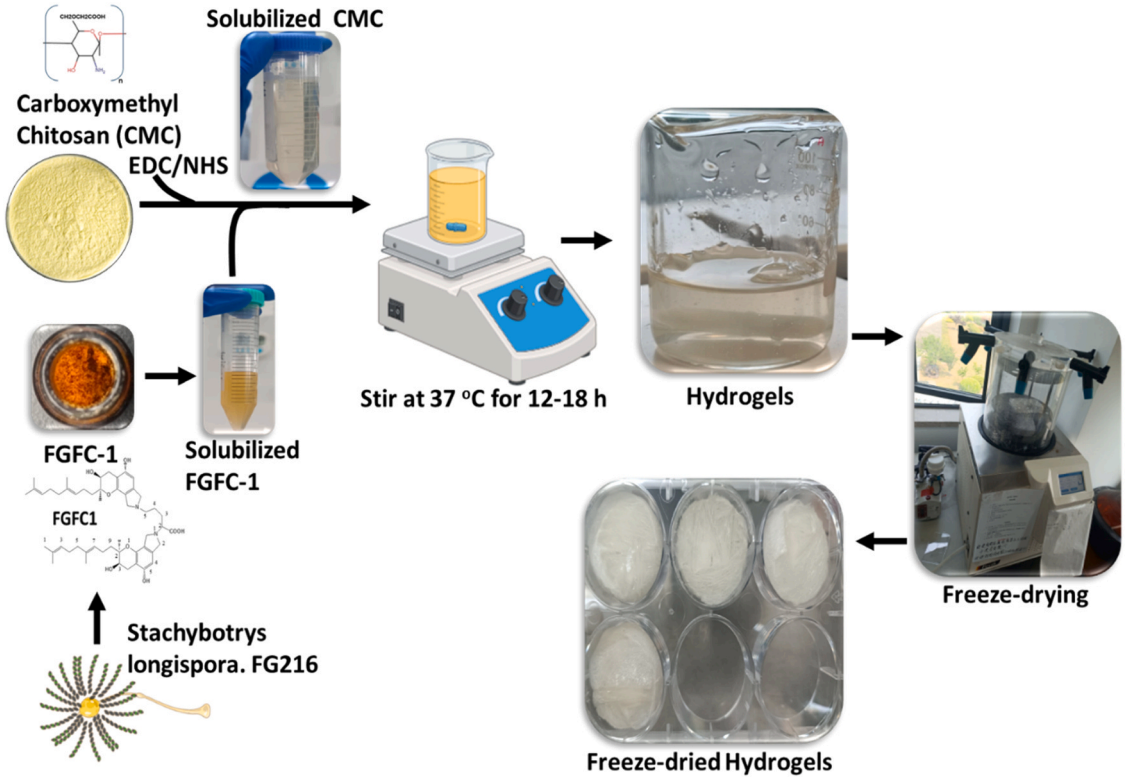

Fig. 1. Steps involved in fabrication process of CMC hydrogels loaded with FGFC-1.

2.3.4. Thermogravimetric analysis (TGA)

The thermal stability of CMC, FGFC-1, and hydrogels was evaluated using a simultaneous thermal analyzer, "NETZSCH TG 209 F1 LIBRA" (Selb, Germany). The samples, weighing approximately 5 mg, were evenly distributed in an alumina crucible and exposed to heating from 20 °C to 500 °C under a nitrogen atmosphere (purity ≥ 99.9 %) at a specified heating rate of 10 °C/min to measure absorption and exothermic curves, as well as thermogravimetric data. An empty aluminum disk served as the reference.

2.3.5. SEM

The microstructural images of freeze-dried samples were examined using a Zeiss Gemini SEM 300, an ultra-high-resolution field emission scanning electron microscope. Briefly, the sample specimens were attached to conductive adhesive tape and then covered with a 10 mA gold layer for 45 seconds using a Quorum SC7620 sputter coater (Quorum Technologies, Lewes, UK). Then, the samples were imaged with a ZEISS Gemini SEM 300 scanning electron microscope (Carl ZEISS Ltd., Oberkochen, Germany). Surface morphology was observed at varying magnifications (100 and 5 μm) with an accelerating voltage of 15 kV.

2.4. Functional properties

2.4.1. Protein adhesion

In order to determine the plasma protein adhesion, the hydrogel samples were incubated in Fetal Bovine Serum (FBS) at 37° C for 4 h [28]. Then, the FBS was removed, and the samples were washed with Phosphate Buffer Saline (PBS) gently twice, followed by staining with Coomassie Brilliant blue (CBB) G-250 for 2 h at 37° C. The excess stain was washed out with a destaining solution containing a methanol-water-acetic acid mixture overnight. The rate of protein absorbed on the hydrogel sample was captured by using a Nikon DXM1200F digital camera.

2.4.2. Mineral adhesion

The mineral binding capacity of hydrogel was assessed using the methodologies described in our previous study[29]. In brief, the hydrogel was immersed in a solution of simulated body fluid for 24 hours, followed by rinsing with phosphate-buffered saline (PBS) to remove any unbound minerals. Subsequently, the mineral bound to the hydrogel was visualized by staining with alizarin red-S, and images were taken using a Nikon DXM1200F digital camera.

2.5. Antibacterial activity

The hydrogel's antibacterial effectiveness was assessed by following our previous methods[30]. Two different bacterial strains, *Escherichia coli* (*E. coli*) (a Gram-negative rod-shaped bacterium) and *Staphylococcus aureus* (S. aureus) (a Gram-positive round-shaped bacterium), were employed to evaluate the antimicrobial properties of the hydrogels. The freeze-dried bacterium vial was diluted in the provided kit supplement (broth and culture plate) and incubated for 24 hours, followed by two additional cultures in standard broth (10 ml per tube). Subsequently, the microbial cultures were utilized for subsequent experiments.

2.5.1. Disc diffusion method

The LB agar culture plates were inoculated with microbial cultures using a sterile bent rod and then punctured in the center with sterile tips (10 μL) for hydrogel samples. Simultaneously, sterile sample discs (Blank Discs- Lot 040921071, Liofilchem SRL, Roseto degli Abruzzi, Italy) were placed on top of the LB agar plates with microbial spread, followed by the addition of different concentrations of FGFC-1 (20 μL) and CMC (20 μL). Tetracycline and chloramphenicol antibiotics (20 μL) were used as positive controls. The zone of inhibition of the samples was measured after 24 hours using an automatic Interscience Scan 500 zone reader (Model:500, 436000S00871, Interscience International, Yvelines, France).

2.5.2. Bacterial cell adhesion

To test the adhesion ability of bacteria, the microbial cultures were treated with FGFC-1, CMC, and hydrogels. The level of bacterial adhesion was then determined using a semiquantitative method through a microbial viability assay (CCK-8) kit. Briefly, *S. aureus* and *E. coli* were grown in a nutrient broth medium. Subsequently, for the bacterial attachment test, 20 μL of samples were combined with 100 μL of bacterial cultures in 48-well culture plates and incubated for 24 hours. After incubation, nonattached bacteria were washed away with PBS. Following this, the CCK-8 staining solution (M4839, AbMole, Houston, TX, USA) was added to each well (1:10, 100 μL) and incubated for three hours in darkness. The absorbance was then read at 450 nm as per the manufacturer's guidelines.

2.6. In vitro cell culture

Mouse bone marrow-derived mesenchymal stem cells (MSCs) were obtained from Shanghai Zhong Qiao Xin Zhou Biotechnology Co., Ltd. (Shanghai, China) and were cultured in mesenchymal stem cell medium (MSCM, Shanghai QiDa Biotechnology Co., Ltd., Shanghai, China) supplemented with 10 % FBS, 1 % p/s, and 1 % mesenchymal stem cell growth supplement (MSCGS). The cells were maintained at 37 °C in a 5 % CO2 incubator (BB 150, Thermo Fisher Scientific, Waltham, MA, USA) and the medium was changed every 2 days. Upon reaching approximately 80 % confluence, the cells were detached using 0.25 % trypsin-EDTA. Cells from passages three to eight were utilized for subsequent experiments.

2.6.1. Proliferation

Cell proliferation was assessed by utilizing a Cell Counting Kit-8 (CCK-8; M4839, AbMole, Houston, TX, USA) following the manufacturer's guidelines. In brief, a 96-well cell culture plate was prepared with CMC (1, 2, and 3 %), FGFC-1 (1 ng, 10 ng, 100 ng, 1 ug, 10 ug, 100 ug, and 1 mg/ml), and hydrogels (HG, HG-0.01, HG-0.1, and HG-1). Subsequently, MSCs were seeded into the designated wells at a concentration of 1×10^4 cells/well with 100 μL of MSCM and incubated for 7 days at 37 °C in a 5 % CO_2 humidified environment. Following the incubation period, the medium was aspirated, cells were washed with PBS, and then 100 μL of medium containing 10 % CCK-8 reagent was added to each well and incubated for 3 hours at 37 °C in a 5 % CO_2 atmosphere without light exposure. Finally, the absorbance at 450 nm was determined using a microplate reader (BioTek, Winooski, VT, USA). The cells without any samples (blank control) served as the 100 % viability reference group.

2.6.2. Cell microstructure

The microstructure of BMMSC cells cultured on hydrogels was visualized through the fluorescence staining method[30]. Briefly, the cells (1×10^4) were mixed with HG, HG-0.01, HG-0.1, and HG-1 and loaded on a culture disc with the medium. Subsequently, the cells were rinsed with PBS and fixed using 4 % paraformaldehyde and 2.5 % glutaraldehyde. Following this, the cell membranes were permeabilized with 0.1 % Triton X-100 before being stained with fluorescence dyes FITC and DAPI according to the standard procedure. To observe the structures of the cells, images were taken using fluorescence microscopy in conjunction with ZEISS Axiocam 305 mono (Axio Vert A1, Serial No. 3847016567, Carl Zeiss Microscopy GmbH, Suzhou, China).

2.6.3. Inflammatory cytokines

To investigate biocompatibility, the cellular inflammatory response was assessed after BMMSCs treatment with hydrogels. BMMSCs were seeded on hydrogels at a cell density of 5×10^5 per well in 48 well plates and cultured with mesenchymal stem cell growth medium and DMEM

medium for 7 days. Following treatment, the cell supernatant collected by centrifugation at 2000 g for 5 minutes and stored at −20° C until use. The levels of cellular cytokines were analyzed using IL-2 and IL-6 ELISA kits. The quantitative measurement of IL-2 and IL-6 was conducted as per the manufacturer's guidelines. Standard curves for IL-2 and IL-6 with varying concentrations were utilized to determine the concentrations of the test samples.

2.7. The effect of hydrogel on bone regeneration

To investigate the effect of hydrogel on bone differentiation, MSCs were cultured on hydrogel with osteogenic differentiation medium along with osteogenic supplements. The control cells were cultured in the same conditions but without hydrogels. In brief, MSCs with a cell density of 5 × 105 were seeded on hydrogels and cultured for 21 days and 27 days, respectively, followed by consecutive analysis.

2.7.1. Osteogenic biomarkers level

In the present study, the possible effect of hydrogels in bone differentiation was confirmed by three staining methods for the bone biomarkers such as osteocalcin and alkaline phosphatase. In brief, the cells were cultured on hydrogels precoated 24 well plates with osteogenic culture medium for 21 and 27 days. Then, they were stained with Alizarin red stain, von kossa stain and alkaline phosphatase stain as per the manufacturers' instructions.

2.7.2. mRNA expression

To examine gene expression, mesenchymal stem cells (MSCs) with a seeding density of 1 × 10^5 cells were cultured in 6-well culture plates that were precoated with hydrogels, for 21 days. The RNA extraction and cDNA synthesis were carried out in accordance with our established protocol [31]. Real-time polymerase chain reaction (RT-PCR) was performed on a 96-well plate utilizing the ABI 7500 Fast Real-Time PCR System (Applied Biosystems, Shanghai, China) with SYBR Green Fast qPCR RT Master Mix (Invitrogen, Shanghai, China). The primers employed for the RT-PCR are listed below.

GAPDH forward 5′ AGC TTG TCA TCA ACG GGA AG3′, GAPDH reverse: 5′ TTT GAT GTT AGT GGG GTC TCG3′

COL I forward:5′GCG AAG GCA ACA GTC GCT3′, COL Ireverse: 5′CTT GGT GGT TTT GTA TTC GAT GAC3′

Osteocalcin (OCN) forward: 5′CTC ACA GAT GCC AAG CCC3′,OCN reverse: 5′CCA AGG TAG CGC CGG AGT CT3′

Alkaline Phosphatase (ALP) forward: 5′ TCC TGA CCA AAA ACC TCA AAG G3′, ALP reverse: 5′TGC TTC ATG CAG AGC CTG C3′

RUNX2 forward: 5′CCA CCA CTC ACT ACC ACA CG3′, RUNX2 reverse: 5′TCA GCG TCA ACA CCA TCA TT3′

2.7.3. Immunocytochemistry

To further confirm the osteogenic stimulatory effect of hydrogel, the cells were differentiated on a hydrogel-coated confocal disc (cat no. 150682, ThermoFisher Scientific) for 21 days. Then, they were fixed with 4 % paraformaldehyde for 30 minutes, permeabilized with 0.1 % Triton™ X-100 for 30 minutes, blocked with 2 % BSA for 1 hour and labeled with 1:100 dilution of primary antibodies (Osteocalcin Polyclonal Antibody, Invitrogen Catalog # BS-4917R and Collagen 1 Polyclonal Antibody, Invitrogen Catalog # BS-10423R) overnight at 4 C followed by incubation with Goat Anti-Rabbit IgG (H+L) FITC conjugated secondary antibody and DyLight 594-conjugated secondary antibody (goat anti-rabbit IgG H&L, Cat No. ab96885, Abcam), respectively, for 2 h at 37 °C. Images were captured using a confocal laser scanning microscope (Leica TCS SP8, Leica Microsystems CMS GmbH, Wetzlar, Germany).

2.8. Statistical analysis

The experiments were carried out with triplicate samples, leading to consistent results. Values are expressed as means ± standard deviation (SD), unless specified differently. One-way ANOVA was employed for statistical analysis and comparisons, with a p-value of less than 0.05 recognized as statistically significant, analyzed using GraphPad Prism 9.4.0 software.

3. Results and discussion

3.1. Physicochemical properties

The porosity and swelling characteristics of the hydrogel are illustrated in Fig. 2. The findings indicate that as the concentration of FGFC-1 increased from 0.001 to 1 mg/ml, the porosity decreased up to 54.29 % from 88.22 %, with the hydrogel containing a high concentration of FGFC-1 (1 mg/ml) exhibiting lower porosity compared to the control hydrogel. Conversely, the swelling capacity of hydrogel was increased by FGFC1 from 132.88. to 157.11 %, but there were not statistically significant. It is hypothesized that the reduction in porosity may be attributed to potential crosslinking interactions between the functional groups of CMC and FGFC-1, as well as the occupation of interstitial spaces within the CMC hydrogels by FGFC-1. Simultaneously, the minimal variations in swelling properties can be explained by the hydrophilic nature of the polymers incorporated in the hydrogel formulation.

Zhu et al. reported that the swelling ratio of chitosan/carboxymethyl cellulose-PEG hydrogels was about 187–315 % based on the CMC concentrations from 1.5 % to 2.5 %, respectively [32]. A recent study demonstrated that composite hydrogels, composed of carboxymethyl cellulose and poly-N-isopropylacrylamide, exhibited reversible swelling when alternately exposed to de-ionized water and NaCl solution [33]. The porosity of the polyurethane porous hydrogel was observed to rise from 53.99 % to 74.67 % as the concentration of CMC increased from 5 % to 10 %. However, at a CMC concentration of 15 %, the porosity decreased to 46.03 % [34]. This indicates that hydrogels containing more than 15 % CMC may not be appropriate for practical applications. Recent studies have emphasized the porosity and swelling properties of CMC hydrogels, indicating that the molecular porosity and mechanical attributes of these hydrogels are critical elements to take into account, as they significantly affect cellular activities [32,33]. Most importantly, research indicates that the porosity of hydrogels affects the movement of nutrients within the matrix and is associated with the swelling behavior and mechanical characteristics of the hydrogel [35].

3.2. In vitro biodegradation

The in vitro biodegradation analysis of hydrogels revealed a consistent pattern across all samples, irrespective of their composition. Interestingly, increasing the concentration of FGFC-1 did not enhance the biodegradation process, even at elevated levels (Fig. 2D). The hydrogels exhibited a gradual degradation process influenced by enzyme lysis and time; specifically, degradation rates decreased from day 1 to day 21, with approximately 50 % degradation occurring between days 6 and 7 across all hydrogels. By the conclusion of the study on day 21, the control hydrogel demonstrated a degradation of approximately 12.94 %, while the hydrogels with a lower FGFC-1 concentration (0.01 mg/ml) showed around 9.52 % degradation. In contrast, hydrogels containing higher concentrations of FGFC-1 (0.1 and 1 mg/ml) exhibited a greater degradation rate compared to those with lower FGFC-1 levels, although their degradation rates were comparable to that of the control hydrogel. Previously, Chen et al. investigated the degradation rate of CMC-OCS-TGF-β3 in PBS for 21 days and found that the degradation rate was comparatively lower in low-molecular-weight heparin- carboxymethyl chitosan (CMC)-oxidized chondroitin sulfate (OCS)-TGF-β3 hydrogels (55.91 %) than CMC-OCS-TGF-β3 (62.62 %) [36]. In the present study, the invitro biodegradation of CMC-HGs was slightly improved by adding FGFC-1 from 0.01 to 1 mg/ml, which may increase susceptibility against proteolytic enzymes.

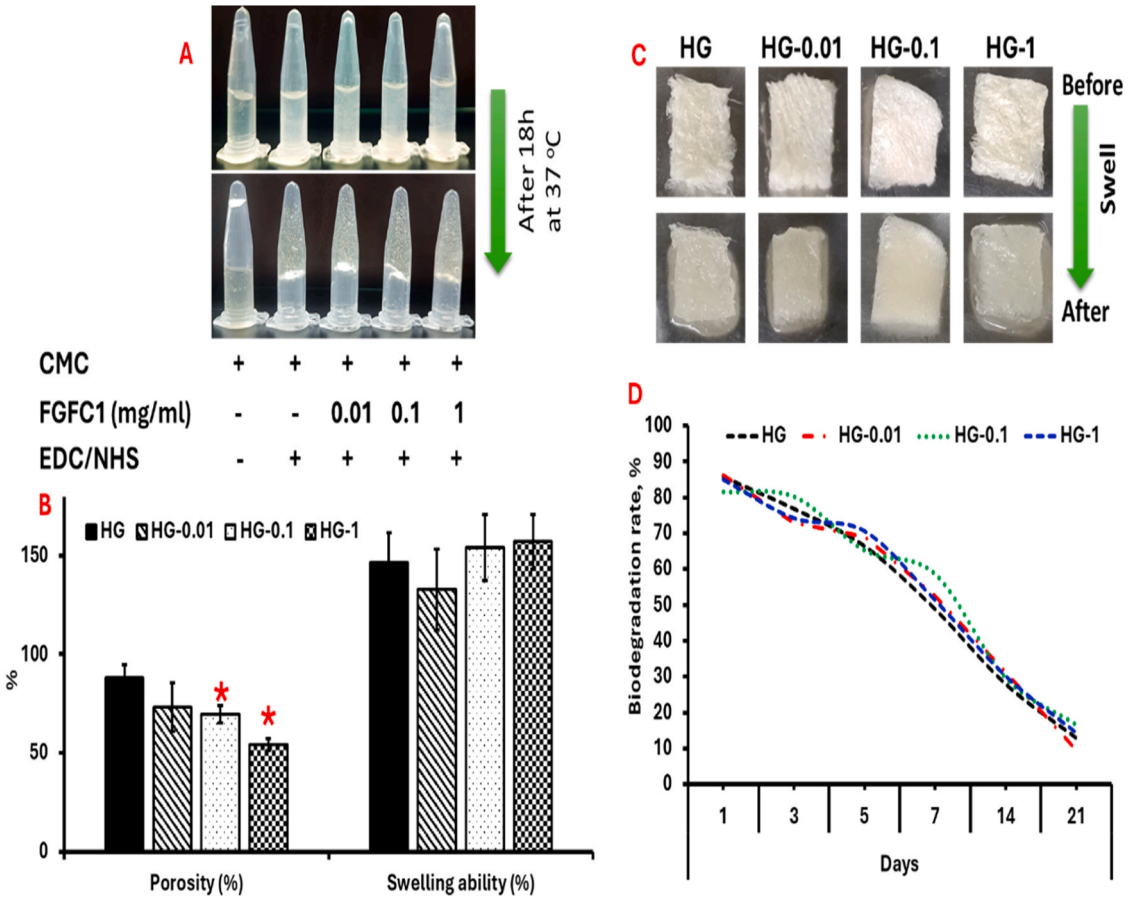

Fig. 2. Porosity, swelling ability and In vitro biodegradation of hydrogels. A- Tubes showing hydrogels after gelation at 37 °C for 18 h, B- porosity and swelling ability of hydrogels, C- representing images of swelling hydrogels before and after incubation, and D- Biodegradation. HG-CMC hydrogels, HG-0.01:- CMC hydrogels with 0.01 mg/ml FGFC-1, HG-0.1:- CMC hydrogels with 0.1 mg/ml FGFC-1 and HG-1:- CMC hydrogels with 1 mg/ml FGFC-1.

3.3. Secondary structural analysis

The secondary structural characteristics of the hydrogel were evaluated using FTIR analysis. To investigate the changes in secondary structure before and after the fabrication of the hydrogel, FTIR analysis was conducted on the raw materials, including CMC and FGFC-1, alongside control hydrogels and FGFC-1-loaded hydrogels (Fig. 3 and Table 1). The findings indicated that the prominent peaks identified in CMC and FGFC-1 were also detectable in the hybrid hydrogels. Notably, the secondary structure of EDC/NHS cross-linked CMC hydrogels exhibited significant alterations when compared to CMC alone, as evidenced by the distinct FTIR patterns of CMC and the CMC hydrogel. Particularly, the unique peak of CMC at 3409.24 cm^{-1} was also observed in FGFC-1-incorporated CMC hydrogels at 3367.02, 3362.8, 3235.39, and 3350.2 cm^{-1} for CMC, CMC-0.01, CMC-0.1, and CMC-1 hydrogels, respectively.

In the present study, the characteristic chitosan peaks at 837.61 cm^{-1} and 1052.12 cm^{-1} represent its saccharide moiety and the major peaks at 1584.06 cm^{-1} and 1308.39 cm^{-1} of CMC corresponded to the vibrational bands related to carboxylates (COO−) asymmetric and symmetric stretches [37]. The peak at 1423.07 cm^{-1} in CMC represented the symmetrical stretching vibration of the carboxylate group, which was shifted from 1404.23 cm^{-1} to 1406.39 cm^{-1} in HGs [38]. The asymmetrical stretching vibrations of the carboxylate group at 1584.06 cm^{-1} were shifted to 1582.51–1585.77 cm^{-1} in HGs, resulting in an intensive band [38]. A typical high intensive band at 2854.25–2920.22 cm^{-1} was observed in FGFC-1, which was not observed in CMC and shifted to the wavenumbers 2875.17 cm^{-1} - 2880.7 cm^{-1} in FGFC-1 loaded HGs. In this study, the presence of a typical peak of FGFC-1 (2854.25–2920.22 cm^{-1}) in FGFC-1-loaded HGs (2875.17 cm^{-1} - 2880.7 cm^{-1}) evidenced the successful fabrication of FGFC-1-loaded CMC hydrogel.

3.4. Microstructure

The microstructure of hydrogels was analyzed in freeze-dried samples through scanning electron microscopy. The results indicated that hydrogels lacking FGFC-1 exhibited a consistent and regular porous microstructure (Fig. 3 B). As the concentration of FGFC-1 increased, the internal microstructure began to change, revealing the formation of micronodules in both surface and cross-sectional views. Conversely, the control hydrogel displayed a more uniform internal structure characterized by interconnected filaments, while higher FGFC-1 concentrations resulted in the appearance of more irregular and flaky filaments. Gonçalves et al. observed a continuous flat irregular rough surface, and well-developed porosities, which were altered to a regular fibrous appearance by the incorporation of other polymers such as hyaluronic acid and silver [39]. Similarly, extensive research has affirmed the inherent porosity of CMC hydrogels, highlighting their capacity to support cellular infiltration and nutrient exchange. Studies have demonstrated that the pore size, distribution, and interconnectivity of these hydrogels play a pivotal role in modulating tissue regeneration, enhancing their applicability in biomedical and tissue engineering fields. Moreover, variations in fabrication techniques and polymer modifications have been shown to influence the structural integrity and functional adaptability of CMC hydrogels, making them a versatile platform for diverse biomedical applications [40–42].

In this study, FGFC-1 induced significant structural modifications in

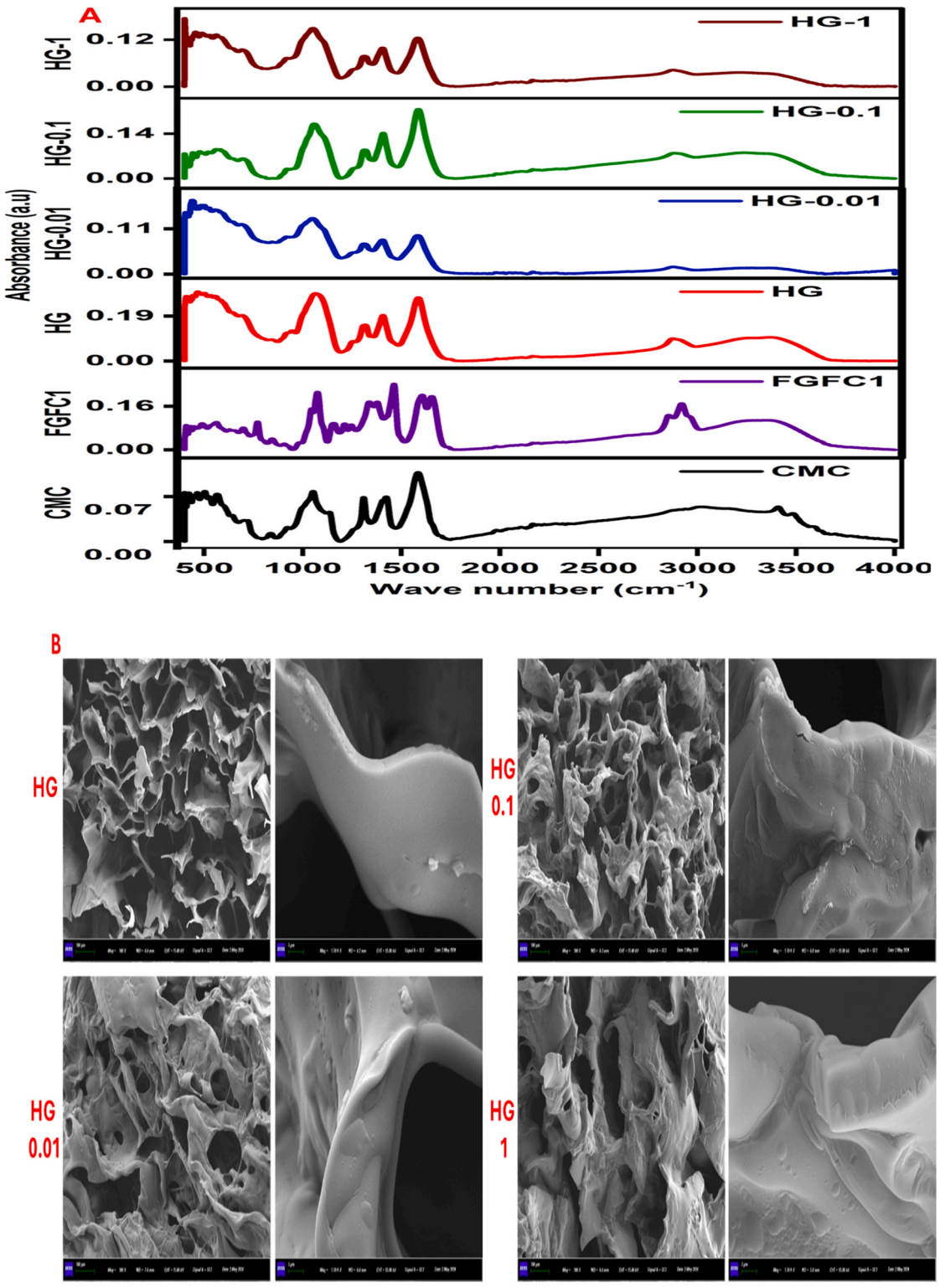

Fig. 3. FTIR spectra (A) and SEM microscopic images (B) of hydrogels. Scale bars 100 μm (100 X) and 5 μm (1.7 KX). HG-CMC hydrogels, HG-0.01:- CMC hydrogels with 0.01 mg/ml FGFC-1, HG-0.1:- CMC hydrogels with 0.1 mg/ml FGFC-1 and HG-1:- CMC hydrogels with 1 mg/ml FGFC-1.

the hydrogels, altering their porosity, surface area, and filament diameter. The average pore sizes for HG, HG-0.01, HG-0.1, and HG-1 were 250.136 μm, 269.284 μm, 240.463 μm, and 172.795 μm, respectively, indicating a reduction in porosity at higher FGFC-1 concentrations. Similarly, the surface area progressively decreased from 204.077 μm^2 in HG to 136.510 μm^2 in HG-0.01, 126.188 μm^2 in HG-0.1, and 101.640 μm^2 in HG-1, suggesting a denser hydrogel network with increasing FGFC-1 levels. The filament diameter ranged from 50.904 to 55.904 μm in HG, 48.074–53.307 μm in HG-0.01, 46.445–51.549 μm in HG-0.1, and 47.355–49.625 μm in HG-1, further illustrating the structural refinement induced by FGFC-1 incorporation. These observations highlight the dose-dependent effects of FGFC-1 on hydrogel

Table 1
Major peaks observed in FTIR spectra of CMC, FGFC-1 and hydrogels.

FTIR Major peaks (Wavenumbers)					
CMC	**FGFC-1**	**HG**	**HG-0.01**	**HG-0.1**	**HG-1**
423.82	489.96	410.67	405.62	443.9	414.34
431.63	562.94	467.31	440.22	478.1	489.62
465.92	698.6	556.84	501.26	560.33	562.58
503.61	770.84	1064.89	1049.11	1058.55	1051.25
565.74	1074.63	1316.3	1310.54	1313.46	1312.25
837.61	1245.39	1406.39	1404.23	1407.44	1404.45
1052.12	1377	1585.77	1582.71	1585.83	1582.51
1308.39	1462	2875.17	2878.1	2880.7	2876.34
1423.07	1605.45	3367.02	3362.8	3235.39	3350.2
1584.06	1653.29				
3015.62	2854.25				
3409.24	2920.22				
	3351.91				

morphology, potentially influencing their functional properties and applicability in biomedical applications.Similar to the present study, Aston et al. observed that alginate hydrogels exhibited a mean pore size ranging from 240 to 170 μm, suggesting their suitability for facilitating nutrient diffusion and cellular infiltration [43].

Similarly, studies on polysaccharide-based hydrogels have reported pore sizes between 250 and 150 μm, reinforcing their ability to support tissue regeneration. The structural characteristics of these hydrogels influence their mechanical strength, permeability, and biocompatibility, making them valuable for biomedical applications. Additionally, poly (ethylene glycol)-grafted superporous hydrogels have been documented with pore sizes ranging from 100 to 250 μm, demonstrating their adaptability for controlled drug delivery and scaffold formation in tissue engineering. The variability in pore size across different hydrogel systems underscores the importance of optimizing structural parameters to achieve specific functional properties. These findings collectively highlight the versatility of hydrogel-based materials in biomedical research, further supporting their integration into tissue engineering and regenerative medicine. [44,45].

In this study, the lyophilized hydrogels exhibited a uniform porous structure with well-balanced porosity, surface area, and filament diameter, optimizing conditions for stem cell culture. The interconnected pore network facilitated efficient nutrient and oxygen diffusion, crucial for sustaining cell viability and proliferation. Supporting these findings, extensive research has emphasized that the porous nature of hydrogels is among the most desirable properties in regenerative medicine. The porosity not only allows for cell infiltration and adhesion but also plays a vital role in mimicking the extracellular matrix, enhancing cellular interactions and differentiation. Additionally, an appropriately tuned pore size can influence mechanical properties, ensuring the structural integrity of the hydrogel while maintaining flexibility for tissue integration. Such features make hydrogels highly valuable in tissue engineering applications, particularly in stem cell-based therapies, where their biocompatibility and ability to support three-dimensional cell growth contribute to effective regeneration and repair processes. The present study further highlights how the controlled porosity of CMC hydrogels strengthens their potential as a platform for advanced biomaterial development [1,45].

3.5. *Thermal stability*

The thermal stability of the raw materials and hydrogels was assessed through TGA analysis, with both TGA and DTG profiles illustrated in Fig. 4. The findings indicated that the DTG of FGFC-1 (71.84 °C) was considerably higher than that of CMC hydrogels (58.4 °C). Nevertheless, the incorporation of FGFC-1 into CMC hydrogels did not lead to a significant enhancement in thermal stability. Overall, the TGA spectra revealed three prominent peaks across all hydrogels, which were associated with moisture loss, the decomposition of organic compounds, and the degradation of the chitosan backbone, respectively [46]. In this

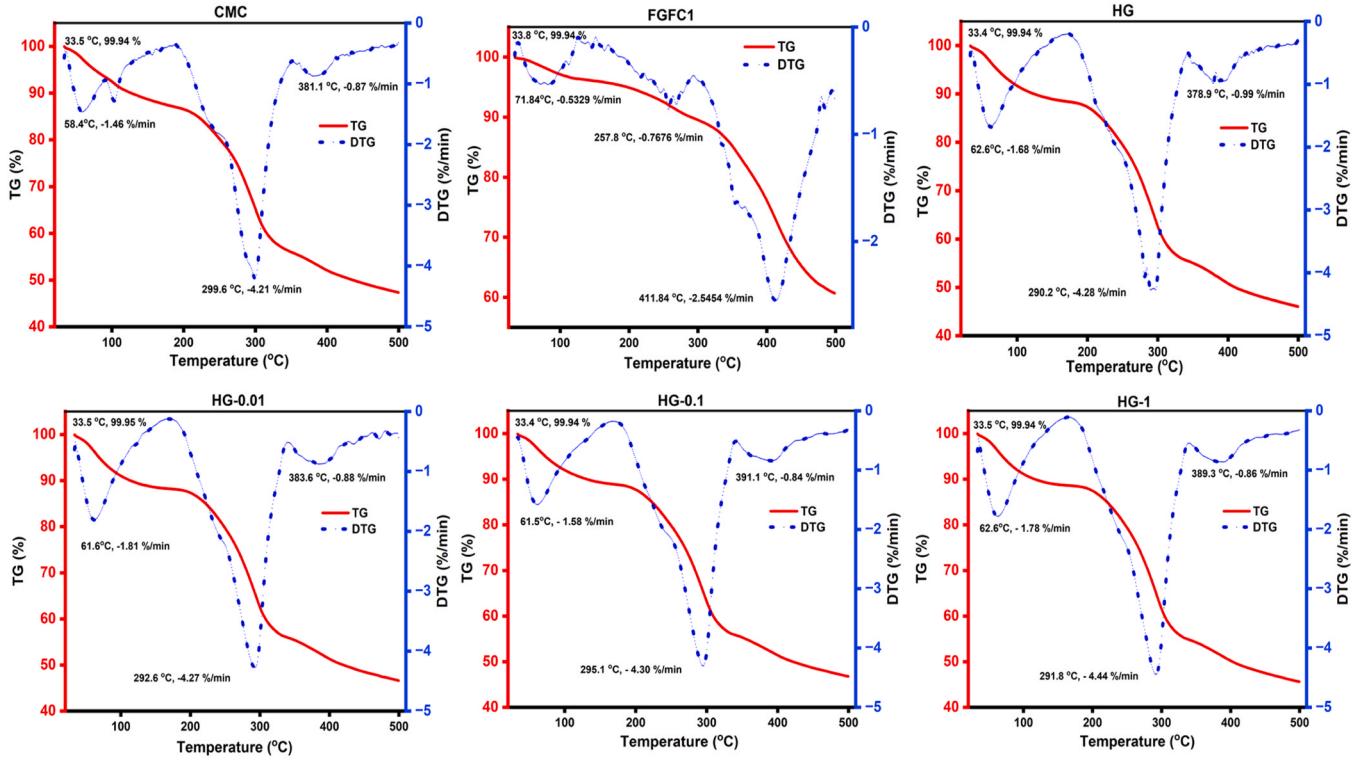

Fig. 4. Thermal degradation profiles (thermogravimetric (TG, red solid line) and derivative thermogravimetry (DTG, blue dotted line)) of raw materials (CMC and FGFC-1) and hydrogels. HG-CMC hydrogels, HG-0.01:- CMC hydrogels with 0.01 mg/ml FGFC-1, HG-0.1:- CMC hydrogels with 0.1 mg/ml FGFC-1 and HG-1:- CMC hydrogels with 1 mg/ml FGFC-1.

study, the main thermal peaks identified between 58.4 and 71.84 °C corresponded to the evaporation of bound water and volatile compounds from both the surface and internal regions of the samples. Furthermore, the intensity of the primary peak was notably higher in the hydrogel samples compared to the raw materials, attributed to their hydrophilic characteristics. The second peak is particularly significant in hydrogels as it indicates the degradation of the chitosan backbone. The second decomposition phase was recorded between 257.8 °C and 299.6 °C, with the thermal stability of the CMC hydrogels (control) at 290.2 °C showing a slight reduction compared to the raw material, which was at 299.6 °C. This decrease can be linked to the compromised structural integrity of CMC upon its transformation into hydrogels. Additionally, the thermal stability of CMC (299.6 °C) was considerably greater than that of FGFC-1 (257.8 °C), which can be attributed to its macromolecular and complex structure. Earlier studies showed that the decomposition temperature of CMC hydrogel was about 180.31–527.32 °C with a reduction in weight exceeding fifty percent of the initial weight [46,47]. Akar et al. opined that the decomposition of CMC during this second stage may result from the degradation of the chitosan backbone and the release of CO_2 as a consequence of decarboxylation [48].

The third peak, which indicates the degradation of any remaining organic and inorganic substances, was slightly lower in the CMC hydrogel than in the CMC (raw material) itself. In contrast, the intensity of the third peak in FGFC-1 was significantly greater than that seen in CMC. The hydrogels incorporating 0.1 FGFC-1 demonstrated a notable prolongation of the third peak's decomposition compared to the CMC control hydrogel.

An earlier study on self-assembled supramolecular pH-responsive CMC-polyoxometalate hydrogels revealed several key thermal degradation points. The first TGA peak for CMC hydrogel, observed at 60 °C, corresponded to a weight loss of approximately 7 %. The second peak, occurring between 240–290 °C, was associated with about 35 % weight loss of CMC due to saccharide ring dehydration and the breakage of glycosidic bonds (C–O–C) in the main polysaccharide chain. The third peak, observed between 300–450 °C, indicated a phase transition from alpha to beta, culminating in the complete decomposition of the hydrogel network at temperatures up to 500 °C. [49]

This study suggests that the enhanced thermal stability of CMC over FGFC-1 can be attributed to its higher crystalline structure and the well-organized configuration of the CMC backbone. Thermogram analysis reveals that the CMC-FGFC-1 hydrogel shows slightly better thermal stability than the CMC hydrogel.

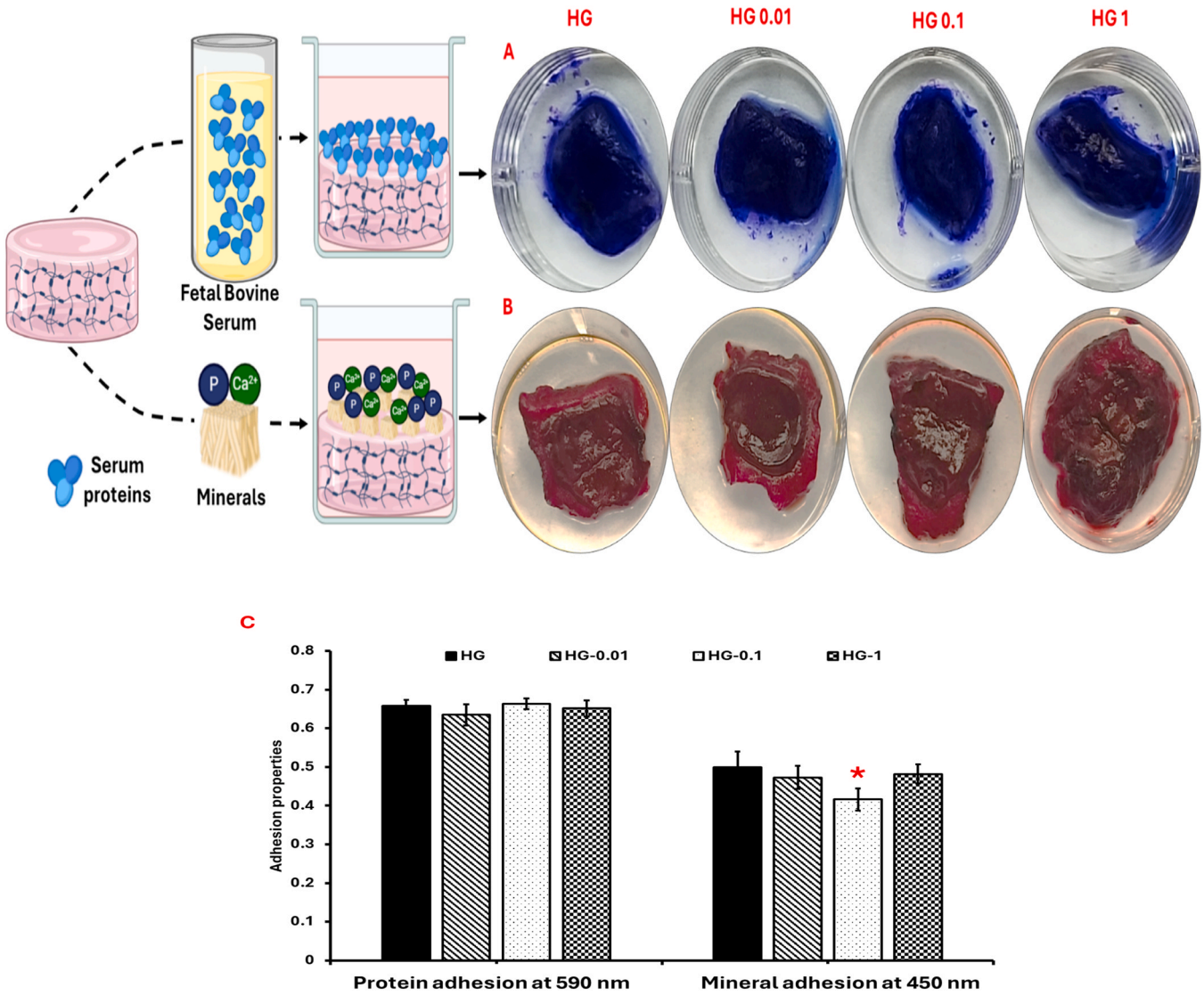

Fig. 5. Functional properties (protein adhesion and Mineral adhesion) of hydrogels. HG-CMC hydrogels, HG-0.01:- CMC hydrogels with 0.01 mg/ml FGFC-1, HG-0.1:- CMC hydrogels with 0.1 mg/ml FGFC-1 and HG-1:- CMC hydrogels with 1 mg/ml FGFC-1.

3.6. Functional properties

The adhesion behaviors of plasma proteins and minerals were utilized to demonstrate the functional characteristics of hydrogels (Fig. 5). The adhesion of plasma proteins reflects the interaction patterns of receptor molecules found in biomaterials. In this study, the presence of FGFC-1 did not affect plasma protein adhesion in hydrogels, and the levels of plasma protein adhesion in the control hydrogels were comparable to those in hydrogels containing FGFC-1 (Fig. 5 A). In contrast to plasma protein adhesion, FGFC-1 influenced the binding behavior of minerals within the hydrogels. Specifically, the mineral adhesion rate in hydrogels loaded with 0.1 mg/ml FGFC-1 was lower (0.416 at 450 nm) than that of the control hydrogels (0.499 at 450 nm); however, no significant differences in mineral adhesion were noted in hydrogels containing 0.01 and 1 mg/ml FGFC-1 when compared to the control (Fig. 5 B).

The surface adhesion characteristics of hydrogels containing plasma proteins can be enhanced through a variety of available surface modification techniques. The distinctive microenvironment of the hydrogel surfaces promotes the interaction and binding of specific molecules [50–52]. At the same time, plasma proteins, including albumin, can interact with hydrogels via multiple mechanisms, such as physical adsorption, electrostatic interactions, hydrogen bonding, and hydrophobic interactions [53,54]. In the field of tissue engineering, improved interaction between plasma proteins would indicate a favorable engagement of hydrogels with cell receptors, which are proteins located

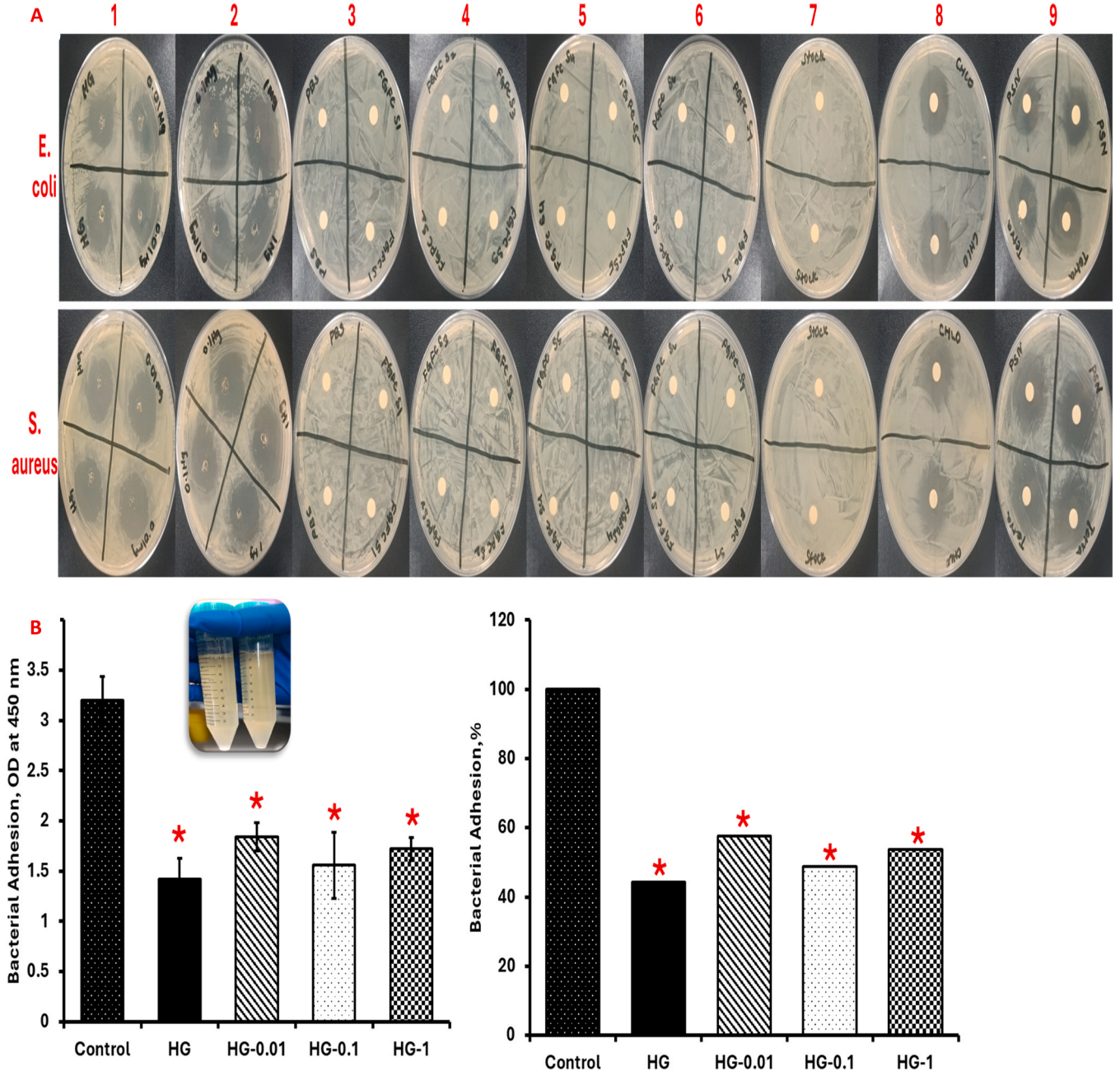

Fig. 6. Antimicrobial activity (*E.coli* and *S. aureus*) of FGFC-1 and CMC hydrogels loaded with different concentrations of FGFC-1. A- disc-diffusion method, B- bacterial adhesion activity (insert- bacteria cultures). 1-control hydrogel and hydrogel with 0.01 mg/ml FGFC-1, 2- hydrogels with 0.1 mg/ml and 1 mg/ml FGFC-1, 3- PBS and 1 ng/ml FGFC-1, 4–10 ng/ml and 100 ng/ml FGFC-1, 5–1 μg/ml and 10 μg/ml FGFC-1, 6–100 μg/ml and 1 mg/ml FGFC-1, 7–5 mg/ml (stock) FGFC-1, 8- standard antibiotic chloramphenicol, 9- standard antibiotics PSN and tetracycline.

within the plasma membrane of cells. Yamada et al. investigated BSA, and FBS-coated peptide (HLT2) hydrogel in Human neonatal dermal fibroblasts growth and found that at least 40 serum proteins were adsorbed onto the surface of the gel via electrostatic interactions, which facilitated protein-mediated cell signalling such as PI3/Akt and MAP-K/ERK pathways [55].

It is reported that hydrogels can adsorb minerals through various mechanisms, including ion exchange, coordination bonds, and van der Waals forces, depending on their functional groups and surface characteristics [56]. Significantly, the structural features of hydrogels resemble the extracellular matrix to facilitate mineral deposition [57,58].

In the present study, the incorporation of FGFC-1 altered the functional properties of hydrogels in mineral adhesion but not in plasma protein adhesion (Fig. 5 C). The actual mechanism of FGFC-1 on mineral adhesion is not known, however, it is believed that its function in altering clot structures and facilitating fibrinolysis could indirectly impact several biological processes related to mineral interactions. For instance, the degradation of fibrin clots can modify the local microenvironment, which may subsequently influence mineral deposition within tissues. In addition, the decreasing pore size, surface area and filament diameter of hydrogels by FGFC1 could also a possible reason to minimize the mineral adhesion rate in HG-1.

3.7. Antimicrobial properties

Two bacterial strains, *E. coli* and S. aureus, were utilized to assess the antimicrobial properties of hydrogels. The effectiveness of these hydrogels was confirmed through disk-diffusion and bacterial cell attachment assays. Antibacterial activity was evaluated by incubating both bacterial strains with varying concentrations of FGFC-1 (1 ng, 10 ng, 100 ng, 1 ug, 10 ug, 100 ug, 1 mg and 5 mg/ml), HG, and FGFC-1-integrated HGs, with comparisons made to positive controls. All four types of hydrogels exhibited antibacterial properties against both *E. coli* and S. aureus, with no significant differences in inhibition among the hydrogels, indicating that the addition of FGFC-1 did not enhance their antibacterial efficacy (Fig. 6). This finding was further supported by experiments where bacteria were incubated with FGFC-1, revealing no inhibitory effect on bacterial growth at any concentration. Notably, the rate of bacterial inhibition was greater in the groups treated with hydrogels compared to controls such as chloramphenicol and PSN. *S. aureus* demonstrated a higher rate of inhibition than *E. coli*, suggesting that *S. aureus* is more susceptible to CMC hydrogels than *E. coli*.

Following the antibacterial disk experiment, we assessed the rate of bacterial cell attachment to hydrogels. The results indicated a significant reduction in bacterial attachment in the groups treated with hydrogels compared to the control group (without hydrogels). Specifically, bacterial attachment decreased from 100 % in the control to between 43.5 % and 65.7 % in the hydrogel-treated groups. The above results concluded that the antibacterial effects of the hydrogels were primarily attributed to CMC rather than FGFC-1. Previous studies have also supported the antibacterial properties of CMC-derived hydrogels. For instance, Venkatesan et al. claimed antibacterial and antifungal activity of CMC hydrogel, especially against *E. coli* and *S. aureus* [3].

Previous research has revealed that secondary metabolites derived from marine fungi may exhibit antioxidant, antimicrobial, antiviral, anti-inflammatory, and anticancer properties [59,60]. On the contrary, no antibacterial activity was observed in FGFC-1-treated groups, which may affected by several factors such as structure, active functional group and susceptibility of secondary metabolites [61,62].

The antibacterial activity of CMC primarily stems from its ability to compromise bacterial membrane integrity through ionogenic groups, particularly positively charged amino groups. These groups disrupt the structural stability of bacterial cells, making them more vulnerable. Additionally, CMC interferes with key cellular processes, such as enzyme activity and DNA synthesis, by chelating metal ions essential for bacterial survival. Beyond these biochemical interactions, the hydrogel network itself acts as a physical barrier, preventing bacterial attachment and proliferation. This multifaceted antibacterial mechanism enhances CMC's potential in biomedical applications [10,63–66].

3.8. Stem cell proliferation

Cell proliferation influenced by hydrogels (HGs) with or without FGFC-1 was assessed by culturing mesenchymal stem cells (MSCs) on HGs for 7 days at 37 °C. The results indicated a significant increase in the proliferation rate of cells cultured on HGs when compared to control cells (without HGs) ($P < 0.05$). Among the various HGs tested, those loaded with 1 mg/ml FGFC-1 (designated as HG-1) demonstrated a notable enhancement in stem cell proliferation compared to the control HG (Fig. 7A). However, no significant changes in cell proliferation rates were observed in HGs containing 0.01 and 0.1 mg/ml FGFC-1 than control HG.

It is well-established that CMC hydrogels play a crucial role in adipose tissue-derived mesenchymal stem cell growth. For instance, encapsulation of MSCs in 2 % CMC hydrogels improved the bioactivity [58]. The stem cell proliferative effect of CMC hydrogel was also upregulated by fabricating with other biomaterials such as gelatine-PEDOT Nanoparticles for neural stem cells [67], oxidized hyaluronic acid for human umbilical cord-derived MSCs [68], gelatin/sodium alginate for bone MSCs [69], platelet-rich plasma-hyaluronic acid/chondrotin sulfate for adipose-derived MSCs [70] and recombinant human collagen I for hUCMSCs [71]. Garrett et al. found that CMC improved cell adhesion, re-epithelialization, and cell migration by engaging with extracellular matrix proteins (fibronectin (3.1-fold) and collagen (9.3-fold)) via its carboxymethyl groups, which further supports cell attachment and proliferation [72].

3.9. Cell adhesion

The morphology of stem cells grown on hydrogels was examined using scanning electron microscopy. In contrast to the control cells cultured on glass slides, which displayed more fibrillar and flattened structures with typical filopodia and lamellipodia characteristics, the stem cells on hydrogels were securely attached and spread across the intramolecular spaces (Fig. 7B). In the control hydrogels, the cells appeared more elongated and were closely interconnected on the surface, completely covering the hydrogels loaded with FGFC-1. Furthermore, the cells formed a more interconnected and complex network, resulting in a more homogeneous tissue-like structure due to the three-dimensional microenvironment provided by the hydrogels.

The adhesion and spreading behavior of stem cells on hydrogels are essential considerations for their use in tissue engineering and regenerative medicine. Stem cells typically demonstrate varying adhesion and spreading behaviors on hydrogels, influenced by material composition, surface modification, mechanical properties and biochemical signals of the biomaterials. In this study, the stem cells exhibited effective attachment and spreading throughout the hydrogels, indicating interpenetrating networks of hydrogels, which was similar to an earlier study reported on gelatin-CMC-sodium alginate hydrogel [73]. He et al. demonstrated that cellular responses such as adhesion, proliferation, differentiation, and cell-cell interactions of stem cells were influenced by the modulation of cationic (amino content) of chitosan [74]. In the present study, HG-1, which exhibited lower porosity, pore size, and filament diameter compared to HG, demonstrated higher cell proliferation and an improved cell adhesion rate. Supporting this observation, an earlier study showed that increasing pore size decreased cell adhesion and the scaffolds with smaller pore size of 96 μm had highest levels of cell attachment [75]. This suggests that specific surface area plays a crucial role in cell adhesion, as hydrogels with larger pores provide less available specific surface area and thus a lower ligand density for initial cell attachment [76,77].

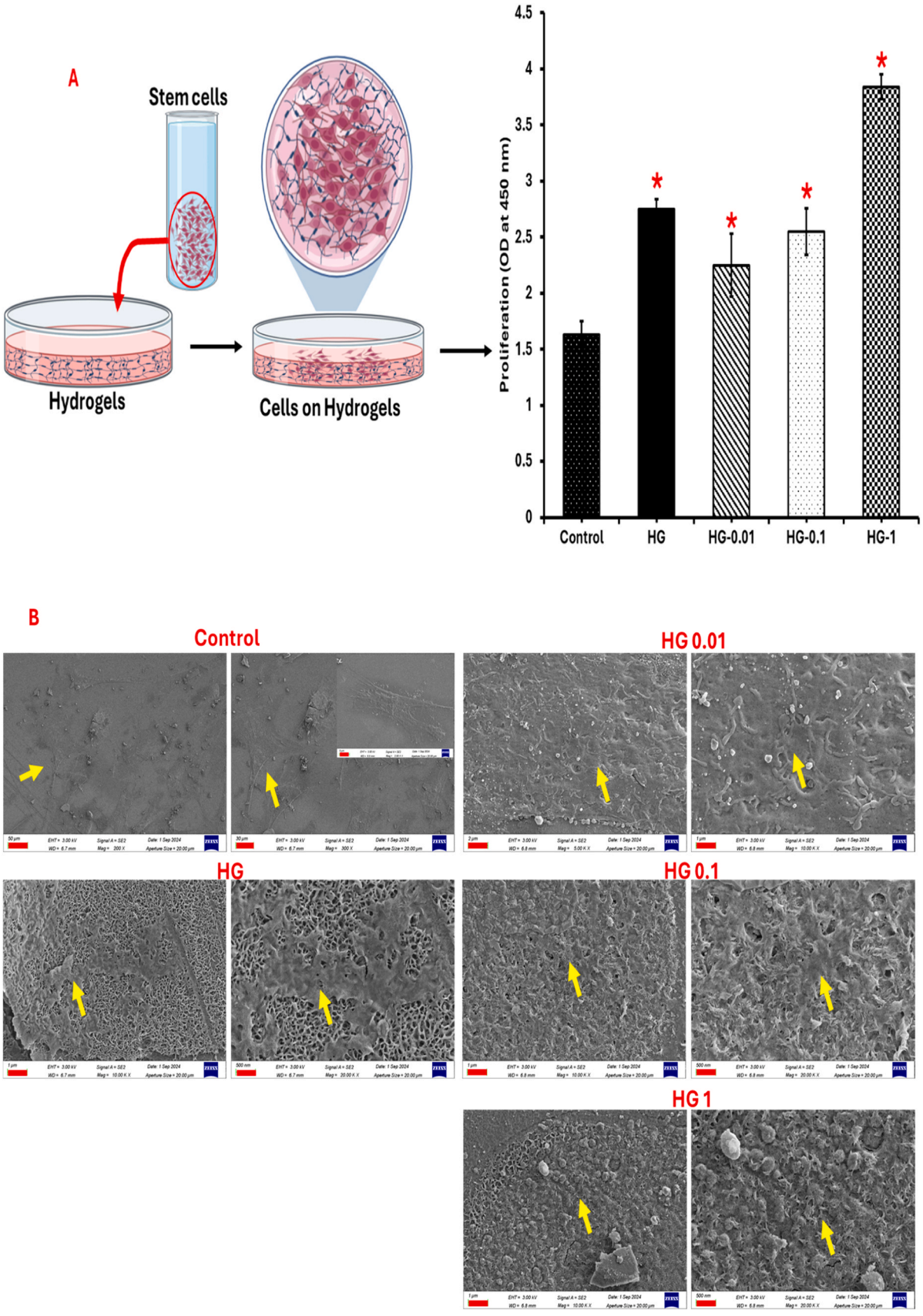

Fig. 7. Cell proliferation (A) and morphological features (B) of stem cells cultured on hydrogels. Control- stem cells without CMC hydrogels, HG-CMC hydrogels, HG-0.01:- CMC hydrogels with 0.01 mg/ml FGFC-1, HG-0.1:- CMC hydrogels with 0.1 mg/ml FGFC-1 and HG-1:- CMC hydrogels with 1 mg/ml FGFC-1. Image B- arrows representing cells on respective samples, insert- morphology of a single stem cell on glass.

3.10. Fluorescence staining

The morphology of stem cells cultured on hydrogel substrates was further assessed using fluorescence staining techniques with FITC and DAPI. Control cells exhibited a distribution across the surface, displaying the characteristic morphology of filopodia and lamellipodia (Fig. 8), which aligned with the observations made through scanning electron microscopy (Fig. 7). Notably, the fluorescence intensity was markedly greater in the hydrogel samples, indicating that the cells were exclusively cultivated on these substrates. The structural framework of the cells was accentuated by FITC, which binds to actin filaments within the cytoskeleton. In this study, the use of FITC and DAPI staining demonstrated the compatibility of cell interactions with the hydrogel surfaces. Specifically, DAPI staining confirmed the predominant distribution of cells on the hydrogels. Similar results were found in MSCs cultured on chitosan-CMC hydrogels and stained with FTIC and DAPI [58]. Severa other studies also confirmed the biocompatibility of CMC hydrogels through FITC/DAPI staining using Human dermal fibroblasts and Human umbilical vein endothelial cells [78]; bone marrow MSCs [79, 80]; primary rabbit corneal epithelial cells [81]; and primary neuronal cells [82]. In this study, the mean FITC and DAPI fluorescence intensities of MSCs increased gradually: 47.95 and 17.85 for control, 66.34 and 24.95 for HG, 72.544 and 29.619 for HG-0.01, 154.831 and 37.237 for HG-0.1 and 109.86 and 42.36 for HG-1, respectively, which proves the proliferative effect of HGs.

In the present study, the higher intensity of fluorescence staining of MSCs justified the stimulatory proliferation ability of CMC hydrogels, which was supported by the cell proliferation results. The results obtained from proliferation, cell adhesion, scanning electron microscopy, and fluorescence staining indicate that FGFC-1-loaded CMC hydrogels exhibit biocompatibility, thereby supporting their potential for facilitating stem cell differentiation.

3.11. Osteogenic stimulatory response

The osteogenic stimulatory effects of HGs were examined using tri-staining techniques, including alizarin red, von Kossa, and ALP staining. Stem cells were subjected to osteogenic differentiation with supplements over periods of 21 and 27 days, both with and without HGs. Generally, cells differentiated for 27 days exhibited stronger positive staining across all three methods compared to those cultured for 21 days (Fig. 9), indicating a higher presence of minerals and ALP expression in the longer culture duration of differentiated bone cells. When comparing the control cells on day 21, those cultured with HGs demonstrated increased intensity in alizarin red and ALP staining, except for the control HG group. However, no significant differences were observed in alizarin red and ALP staining intensity between the control and HG groups, or between control-HG and FGFC-1-HGs on day 27. Like the alizarin red results, von Kossa staining intensity was greater in HGs compared to control cells, and this intensity increased with higher concentrations of FGFC-1 on both days 21 and 27.

Notably, elevating FGFC-1 concentrations from 0.01 to 1 mg/ml enhanced the osteogenic behavior of differentiated cells cultured on HGs, resulting in greater staining intensity in cells treated with HG-1.

3.11.1. mRNA expression

To further validate the osteogenic stimulatory effect of HGs, the levels of osteogenic mRNA in differentiated stem cells were measured. The expression of collagen mRNA was elevated in control HG, HG-0.1, and HG-1 when compared to the control group (Fig. 10). However, the expression of osteocalcin mRNA did not show significant changes in HG-cultured cells relative to control cells, except for HG-1. Conversely, the addition of 0.1 and 1 mg/ml FGFC-1 notably enhanced ALP mRNA expression compared to the control, while 0.01 mg/ml FGFC-1 and control HGs did not significantly affect ALP mRNA levels. Notably, RUNX2 mRNA expression was significantly increased by FGFC-1 across

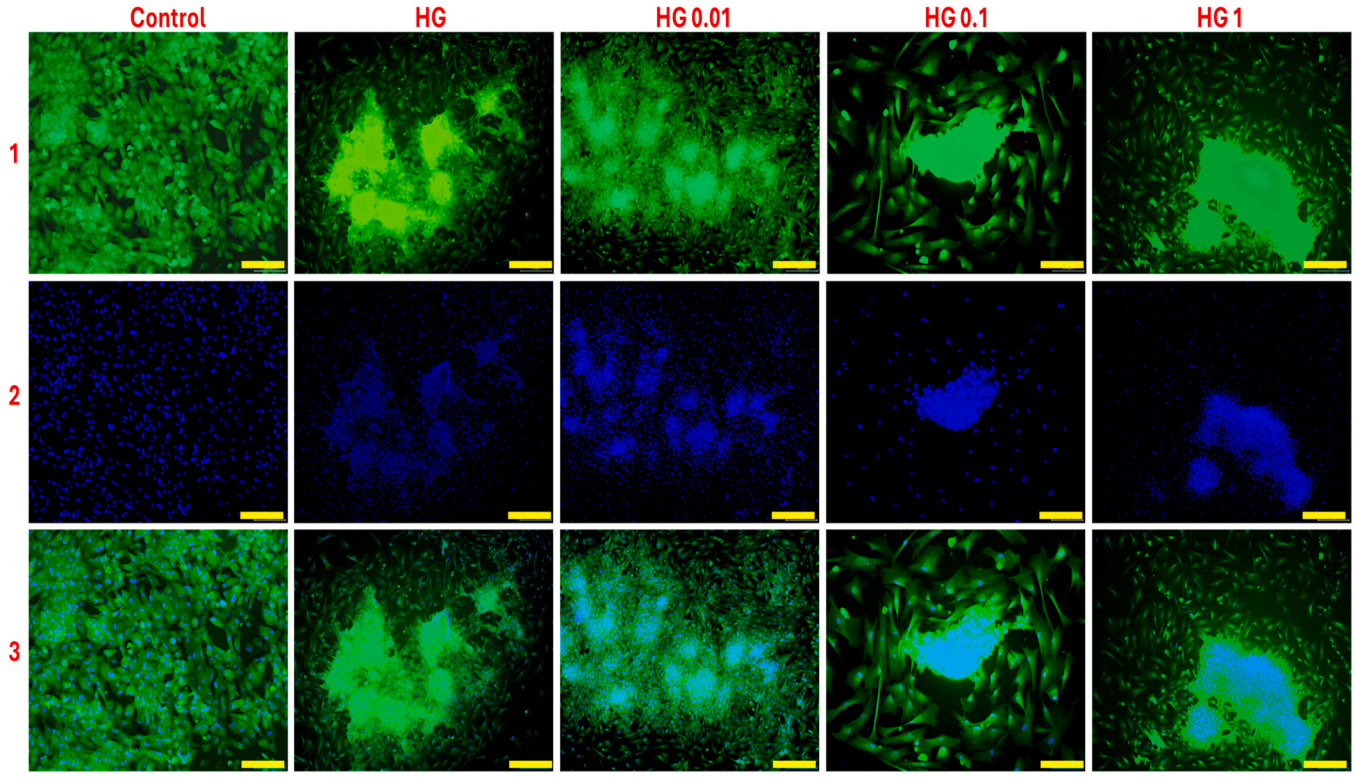

Fig. 8. Fluorescence staining images of stem cells cultured on CMC hydrogels loaded with FGFC-1. Images 1, 2 and 3: Green (FITC), and blue (DAPI) fluorophores-stained stem cells and Merged images, respectively. Scalebar- 500 μm. Control- stem cells without CMC hydrogels, HG-CMC hydrogels, HG-0.01:- CMC hydrogels with 0.01 mg/ml FGFC-1, HG-0.1:- CMC hydrogels with 0.1 mg/ml FGFC-1 and HG-1:- CMC hydrogels with 1 mg/ml FGFC-1.

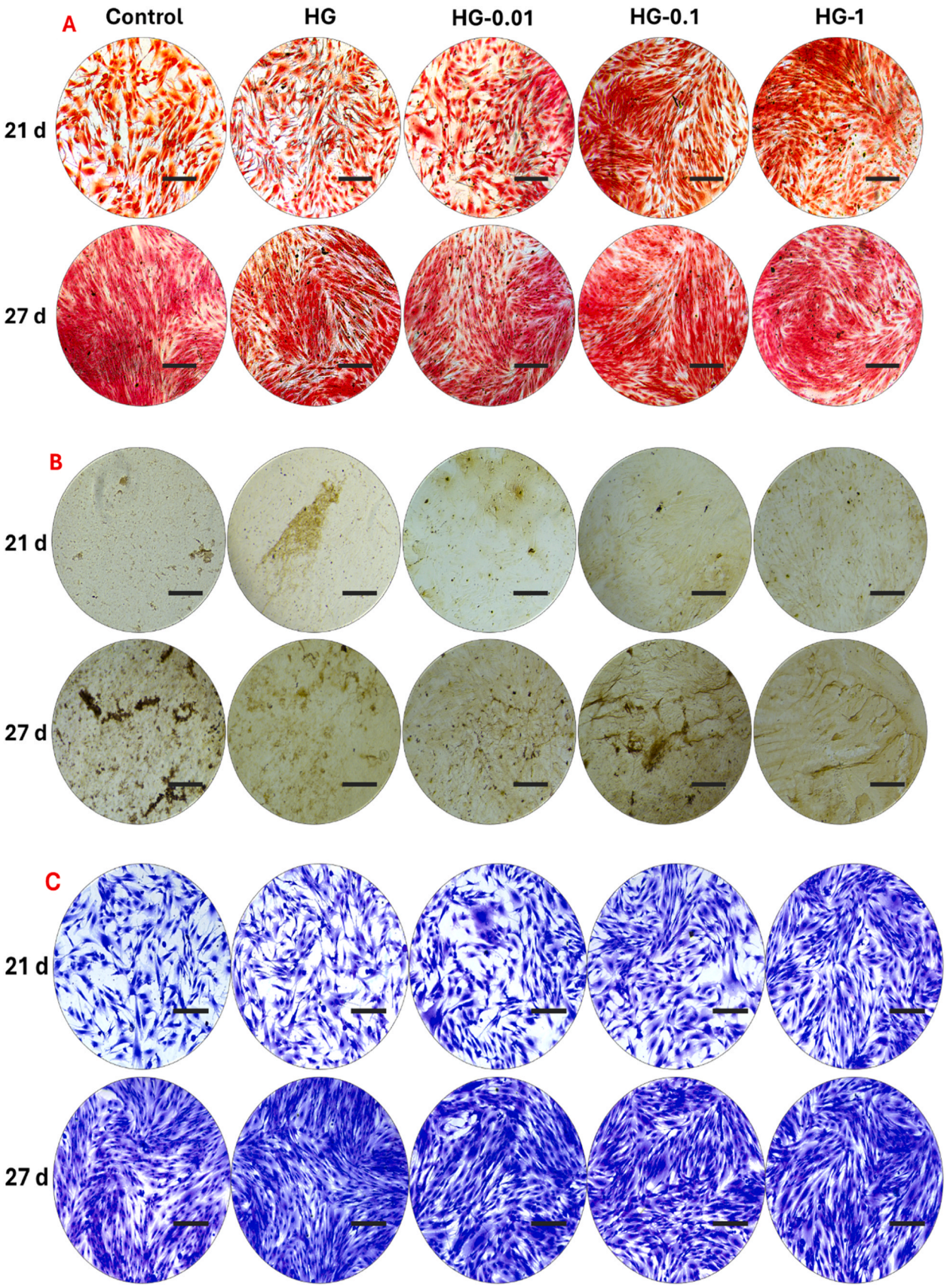

Fig. 9. Alizarin red (A), von Kossa (B) and alkaline phosphatase (C) staining of differentiated MSCs cultured on CMC hydrogels with FGFC-1 for 21 days and 27 days. Scalebar-200 μm. Control- stem cells without CMC hydrogels, HG-CMC hydrogels, HG-0.01:- CMC hydrogels with 0.01 mg/ml FGFC-1, HG-0.1:- CMC hydrogels with 0.1 mg/ml FGFC-1 and HG-1:- CMC hydrogels with 1 mg/ml FGFC-1.

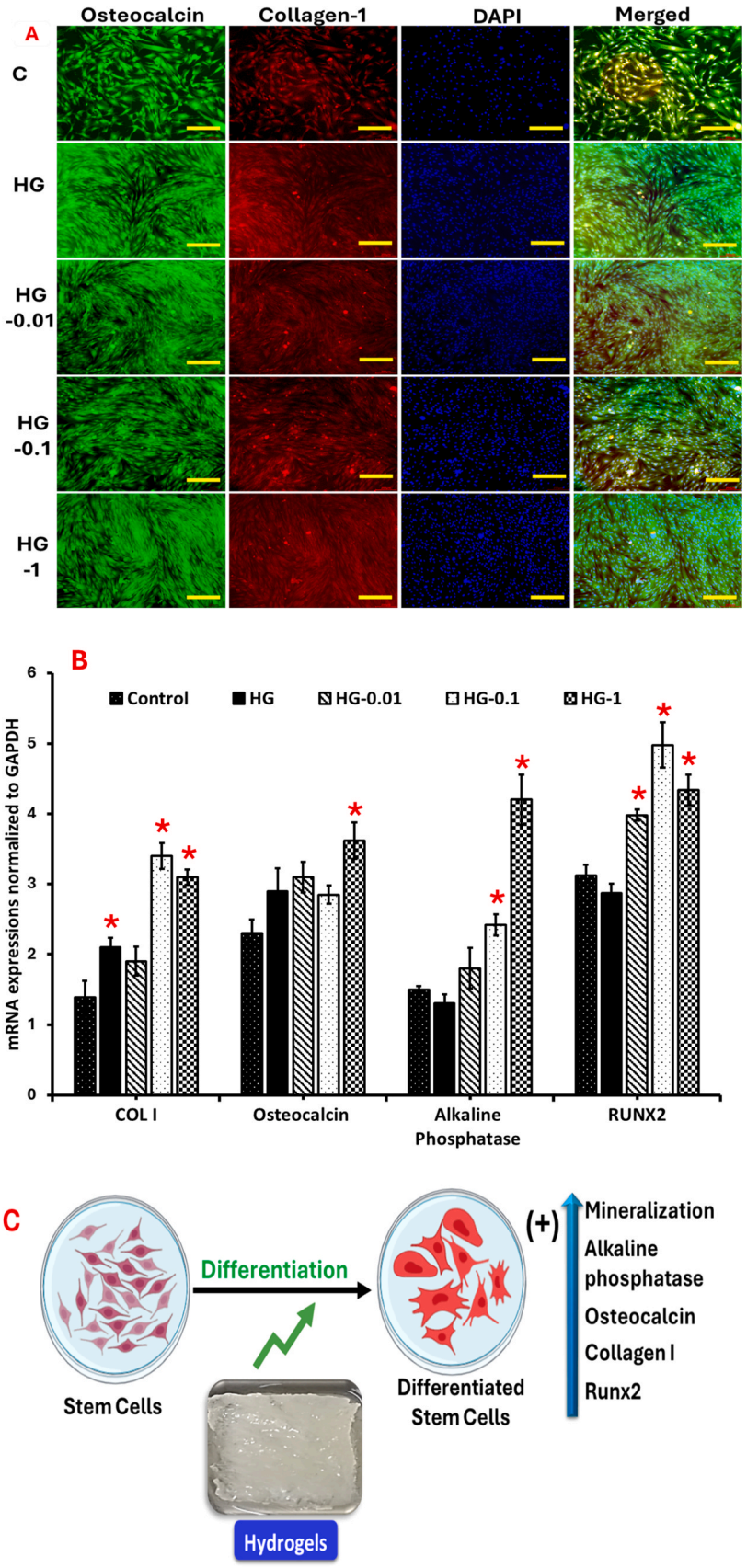

(caption on next page)

Fig. 10. Immunocytochemistry (A), mRNA expression (B) of differentiated stem cells cultured on CMC-hydrogels and the illustration representing the role of FGFC-1 loaded CMC hydrogels in osteogenic differentiation of stem cells (C). C- stem cells without CMC hydrogels, HG-CMC hydrogels, HG-0.01:- CMC hydrogels with 0.01 mg/ml FGFC-1, HG-0.1:- CMC hydrogels with 0.1 mg/ml FGFC-1 and HG-1:- CMC hydrogels with 1 mg/ml FGFC-1. Scalebar-200 μm. Cells were incubated with Osteocalcin Polyclonal Antibody or Collagen 1 Polyclonal Antibody followed by incubation with Goat Anti-Rabbit IgG (H+L) FITC conjugated secondary antibody (Green) or DyLight 594-conjugated secondary antibody (red), respectively.

all HGs in comparison to control cells, a trend that was not observed in the control HGs. To support this evidence, earlier studies claimed that the CMC hydrogels fabricated with sodium alginate, carboxymethyl cellulose, chitosan and magnesium phosphate enhanced the osteogenic gene expression of MSCs [58,83–85].

3.12. Immunocytochemistry

The investigation into the capacity of hydrogels (HGs) to enhance the expression of osteocalcin and collagen-1 in differentiated stem cells was conducted using immunocytochemistry (Fig. 10)

Overall, the differentiated stem cells exhibited positive expression of osteocalcin (Green) and collagen-1 (Red) across all groups, which clearly indicated successful differentiation into bone cells. Notably, the intensity of both green and red staining increased as the concentration of FGFC-1 was raised from 0.01 to 1 mg/ml in the HGs. However, no significant differences were noted between the control HG and those with FGFC-1 concentrations of 0.01 and 0.1 mg/ml. Interestingly, the staining intensity was markedly higher in cells cultured on HGs compared to the control. These findings convincingly demonstrate that HGs promote the expression of bone biomarkers, such as osteocalcin and collagen-1, more effectively than the control conditions.

Similar to the present study, Arab-Ahmadi et al. reported the osteogenic stimulatory effect in human bone marrow MSC cultured on CMC fabricated with cobalt-loaded laponite- polycaprolactone nanofiber [86]. In another study, Zhao et al. found CMC nanofibers fabricated with simulated body fluid (SBF)-based biomimetic mineralization (hydroxyapatite) improved the osteogenic activity of mouse bone marrow stromal cells by increasing Runx2, OCN and ALP gene expression [87]. The adipose tissue-derived mesenchymal stem cells encapsulation in 2 % CMC and 2 % chitosan (50:50 ratio) could trigger early osteogenesis and also accelerated differentiation to the maturity phase of osteoblasts without the use of external osteogenic differentiation agents [58]. Earlier, the CMC hydrogels fabricated with gelatin and PEDOT nanoparticles stimulated the differentiation of neural stem cells [67]. There are several key signaling mechanisms of CMC in the osteogenic differentiation of stem cells such as mimicking the natural extracellular matrix (Extracellular Matrix Mimicry) behavior, accelerating growth factors other biochemical cues that promote specific differentiation pathways, such as osteogenic (bone) or chondrogenic (cartilage) differentiation, tailoring architectural properties like porosity and stiffness to satisfy the requirements for stem cells optimal growth conditions and modulating regenerative signals through stem cells and the ECM components interactions [58,88]. In the present study, the increased mineral adhesion behavior of CMC and FGFC-1 also justified the osteogenic stimulatory effect of FGFC-1-loaded CMC hydrogels.

4. Conclusion

This study comprehensively examined the impact of FGFC-1 on CMC hydrogels, revealing significant modifications in their functional, structural, and biological properties. FGFC-1 altered mineral adhesion and biodegradation while maintaining swelling behavior and protein adhesion. Microscopic analysis showed that higher FGFC-1 concentrations reduced porosity, whereas lower doses did not affect hydrogel morphology. Although FGFC-1 did not exhibit direct antimicrobial activity, its incorporation into CMC hydrogels significantly improved their antibacterial properties against E. coli and S. aureus. Importantly, FGFC-1 promoted stem cell proliferation, particularly at 1 mg/ml, fostering biomimetic growth patterns. Higher FGFC-1 doses enhanced the osteogenic potential of CMC hydrogels by increasing mineral expression and key osteogenic markers such as collagen I, osteocalcin, alkaline phosphatase, and RUNX2. These findings suggest FGFC-1, derived from marine fungi, holds promise for developing biomaterials in bone tissue engineering.

While this study demonstrates the promising role of FGFC-1 in enhancing the biological properties of CMC hydrogels, its influence on swelling behavior and protein adhesion was found to be negligible, indicating potential limitations in hydrogel tunability. Moreover, FGFC-1 alone did not exhibit antimicrobial activity against E. coli and S. aureus, emphasizing the need for further investigation across a broader range of bacterial strains, including both Gram-positive and Gram-negative pathogens, to better assess its antimicrobial potential and biomedical applications.

CRediT authorship contribution statement

Jeevithan Lakshmi: Writing – original draft, Investigation. **Shuyue Wang:** Investigation, Formal analysis. **Thomas Sabu:** Writing – review & editing, Validation. **Jose Eduardo Mate Sanchez de Val:** Writing – review & editing, Supervision. **Wu Wenhui:** Writing – original draft, Supervision, Conceptualization. **Elango Jeevithan:** Writing – review & editing, Supervision, Conceptualization.

Declaration of Competing Interest

The authors declare that they have no known competing financial interests or personal relationships that could have appeared to influence the work reported in this paper.

Acknowledgments

W.W acknowledges funding from SciTech Funding by CSPFTZ Lingang Special Area Marine Biomedical Innovation Platform, China and the National Natural Science Foundation of China (No. 82173731), China. J.E thanks partially funding through the PVARETINOL Project by CASTANEA INVESTIGACIONES AGRUPACIÓN DE INTERÉS ECONÓMICO and its participants under the call "Financiación estructurada de proyectos de I + D por Agrupaciones de Interés Económico (A. I.E.)," in collaboration with INVENTIUM.

Supplementary material

Supplementary Fig. S1. Molecular structure of Carboxymethyl chitosan ((C8H13NO6)n(C8H13NO5)m)). Supplementary Fig. S2. Cell viability of bone marrow mesenchymal stem cells treated with different concentrations of CMC (1,2 and 3 %) (A) and FGFC1 (1 ng, 10 ng, 100 ng, 1 ug, 10 ug, 100 ug 1 mg/ml and 5 mg/ml) (B).

Appendix A. Supporting information

Supplementary data associated with this article can be found in the online version at doi:10.1016/j.biopha.2025.118162.

References

[1] M.C. Catoira, L. Fusaro, D. Di Francesco, M. Ramella, F. Boccafoschi, Overview of natural hydrogels for regenerative medicine applications, J. Mater. Sci: Mater. Med 30 (2019) 115, https://doi.org/10.1007/s10856-019-6318-7.

[2] S.A. Khan, L.A. Shah, M. Shah, I. Jamil, Engineering of 3D polymer network hydrogels for biomedical applications: a review, Polym. Bull. 79 (2022) 2685–2705, https://doi.org/10.1007/s00289-021-03638-5.
[3] A. Jayakumar, V.K. Jose, J. Lee, Hydrogels for medical and environmental applications, Small Methods 4 (2020) 1900735, https://doi.org/10.1002/smtd.201900735.
[4] S. Adepu, S. Ramakrishna, Controlled drug delivery systems: current status and future directions, Molecules 26 (2021) 5905, https://doi.org/10.3390/molecules26195905.
[5] V. Gounden, M. Singh, Hydrogels and wound healing: current and future prospects, Gels 10 (2024) 43, https://doi.org/10.3390/gels10010043.
[6] G. Chakrapani, M. Zare, S. Ramakrishna, Intelligent hydrogels and their biomedical applications, Mater. Adv. 3 (2022) 7757–7772, https://doi.org/10.1039/D2MA00527A.
[7] V.K. Mourya, N.N. Inamdara, Ashutosh Tiwari, Carboxymethyl chitosan and its applications, Adv. Mater. Lett. 1 (2010) 11–33, https://doi.org/10.5185/amlett.2010.3108.
[8] L. Upadhyaya, J. Singh, V. Agarwal, R.P. Tewari, Biomedical applications of carboxymethyl chitosans, Carbohydr. Polym. 91 (2013) 452–466, https://doi.org/10.1016/j.carbpol.2012.07.076.
[9] Y. Geng, H. Xue, Z. Zhang, A.C. Panayi, S. Knoedler, W. Zhou, B. Mi, G. Liu, Recent advances in carboxymethyl chitosan-based materials for biomedical applications, Carbohydr. Polym. 305 (2023) 120555, https://doi.org/10.1016/j.carbpol.2023.120555.
[10] Z. Shariatinia, Carboxymethyl chitosan: Properties and biomedical applications, Int. J. Biol. Macromol. 120 (2018) 1406–1419, https://doi.org/10.1016/j.ijbiomac.2018.09.131.
[11] P.V. Bramhachari, S. Anju, G.M. Sheela, T.R. Komaraiah, P. Venkataiah, A.M.V. N. Prathyusha, Secondary Metabolites from Marine Endophytic Fungi: Emphasis on Recent Advances in Natural Product Research, in: B.P. Singh (Ed.), Advances in Endophytic Fungal Research, Springer International Publishing, Cham, 2019, pp. 339–350, https://doi.org/10.1007/978-3-030-03589-1_15.
[12] W.-S. Shu, L.-N. Huang, Microbial diversity in extreme environments, Nat. Rev. Microbiol 20 (2022) 219–235, https://doi.org/10.1038/s41579-021-00648-y.
[13] M. Conte, E. Fontana, A. Nebbioso, L. Altucci, Marine-derived secondary metabolites as promising epigenetic bio-compounds for anticancer therapy, Mar. Drugs 19 (2020) 15, https://doi.org/10.3390/md19010015.
[14] T. Li, T. Ding, J. Li, Medicinal purposes: bioactive metabolites from marine-derived organisms, MRMC 19 (2018) 138–164, https://doi.org/10.2174/1389557517666170927113143.
[15] X. Li, H. Xu, Y. Li, S. Liao, Y. Liu, Exploring diverse bioactive secondary metabolites from marine microorganisms using co-culture strategy, Molecules 28 (2023) 6371, https://doi.org/10.3390/molecules28176371.
[16] I.J. Macha, B. Ben-Nissan, W.H. Müller, Marine-Based Biomaterials for Tissue Engineering Applications, in: A.H. Choi, B. Ben-Nissan (Eds.), Marine-Derived Biomaterials for Tissue Engineering Applications, Springer Singapore, Singapore, 2019, pp. 99–111, https://doi.org/10.1007/978-981-13-8855-2_5.
[17] A. Sugumaran, R. Pandiyan, P. Kandasamy, M.G. Antoniraj, I. Navabshan, B. Sakthivel, S. Dharmaraj, S.K. Chinnaiyan, V. Ashokkumar, C. Ngamcharussrivichai, Marine biome-derived secondary metabolites, a class of promising antineoplastic agents: a systematic review on their classification, mechanism of action and future perspectives, Sci. Total Environ. 836 (2022) 155445, https://doi.org/10.1016/j.scitotenv.2022.155445.
[18] M.L. Ciavatta, F. Lefranc, L.M. Vieira, R. Kiss, M. Carbone, W.A.L. Van Otterlo, N. B. Lopanik, A. Waeschenbach, The phylum bryozoa: from biology to biomedical potential, Mar. Drugs 18 (2020) 200, https://doi.org/10.3390/md18040200.
[19] H. Safavi-Hemami, S.E. Brogan, B.M. Olivera, Pain therapeutics from cone snail venoms: from ziconotide to novel non-opioid pathways, J. Proteom. 190 (2019) 12–20, https://doi.org/10.1016/j.jprot.2018.05.009.
[20] R. Guo, Y. Zhang, D. Duan, Q. Fu, X. Zhang, X. Yu, S. Wang, B. Bao, W. Wu, Fibrinolytic evaluation of compounds isolated from a marine fungus *Stachybotrys longispora* FG216, Chin. J. Chem. 34 (2016) 1194–1198, https://doi.org/10.1002/cjoc.201600623.
[21] L. Jeevithan, X. Diao, J. Hu, J. Elango, W. Wu, J.E. Mate Sanchez De Val, S. Rajendran, T. Sundaram, S.K. Rajamani Sekar, Recent advancement of novel marine fungi derived secondary metabolite fibrinolytic compound FGFC in biomedical applications: a review, Front. Cell. Infect. Microbiol 14 (2024) 1422648, https://doi.org/10.3389/fcimb.2024.1422648.
[22] S. Yan, B. Zhang, J. Feng, H. Wu, N. Duan, Y. Zhu, Y. Zhao, S. Shen, K. Zhang, W. Wu, N. Liu, FGFC1 selectively inhibits erlotinib-resistant non-small cell lung cancer via elevation of ROS mediated by the EGFR/PI3K/Akt/mTOR Pathway, Front. Pharm. 12 (2022) 764699, https://doi.org/10.3389/fphar.2021.764699.
[23] G. Wang, W. Wu, Q. Zhu, S. Fu, X. Wang, S. Hong, R. Guo, B. Bao, Identification and fibrinolytic evaluation of an isoindolone derivative isolated from a rare marine fungus *Stachybotrys longispora* FG216, Chin. J. Chem. 33 (2015) 1089–1095, https://doi.org/10.1002/cjoc.201500176.
[24] Y.D. Nokoorani, A. Shamloo, M. Bahadoran, H. Moravvej, Fabrication and characterization of scaffolds containing different amounts of allantoin for skin tissue engineering, Sci. Rep. 11 (2021) 16164, https://doi.org/10.1038/s41598-021-95763-4.
[25] Z.B.Z. Shawon, M.R. Khan, N.A. Takia, T.H. Khan, A. Rahman, M.E. Hoque, Structure-property-function relationships of sustainable hydrogels, in: Sustainable Hydrogels, Elsevier, 2023, pp. 79–111, https://doi.org/10.1016/B978-0-323-91753-7.00017-X.
[26] J.A. Jennings, Controlling chitosan degradation properties in vitro and in vivo, in: Chitosan Based Biomaterials Volume 1, Elsevier, 2017, pp. 159–182, https://doi.org/10.1016/B978-0-08-100230-8.00007-8.
[27] L. Tao, L. Zhonglong, X. Ming, Y. Zezheng, L. Zhiyuan, Z. Xiaojun, W. Jinwu, *In vitro* and *in vivo* studies of a gelatin/carboxymethyl chitosan/LAPONITE® composite scaffold for bone tissue engineering, RSC Adv. 7 (2017) 54100–54110, https://doi.org/10.1039/C7RA06913H.
[28] J. Elango, R. Bushin, A. Lijnev, P.N. De Aza, C.P.-A. Martínez, J.M.G. Marín, A. B. Hernandez, L.R.M. Olmo, J.E.M.S.D. Val, The effect of germanium-loaded hydroxyapatite biomaterials on bone marrow mesenchymal stem cells growth, Cells 11 (2022) 2993, https://doi.org/10.3390/cells11192993.
[29] J. Elango, C. Zamora-Ledezma, F. Alexis, W. Wu, J.E. Maté-Sánchez De Val, Protein adsorption, calcium-binding ability, and biocompatibility of silver nanoparticle-loaded polyvinyl alcohol (PVA) hydrogels using bone marrow-derived mesenchymal stem cells, Pharmaceutics 15 (2023) 1843, https://doi.org/10.3390/pharmaceutics15071843.
[30] J. Elango, C. Zamora-Ledezma, D. Negrete-Bolagay, P.N.D. Aza, V.M. Gómez-López, I. López-González, A. Belén Hernández, J.E.M.S. De Val, W. Wu, Retinol-loaded poly(vinyl alcohol)-based hydrogels as suitable biomaterials with antimicrobial properties for the proliferation of mesenchymal stem cells, IJMS 23 (2022) 15623, https://doi.org/10.3390/ijms232415623.
[31] J. Elango, J. Robinson, J. Zhang, B. Bao, N. Ma, J.E.M.S. De Val, W. Wu, Collagen peptide upregulates osteoblastogenesis from bone marrow mesenchymal stem cells through MAPK- Runx2, Cells 8 (2019) 446, https://doi.org/10.3390/cells8050446.
[32] H. Zhu, S. Chen, H. Duan, J. He, Y. Luo, Removal of anionic and cationic dyes using porous chitosan/carboxymethyl cellulose-PEG hydrogels: Optimization, adsorption kinetics, isotherm and thermodynamics studies, Int. J. Biol. Macromol. 231 (2023) 123213, https://doi.org/10.1016/j.ijbiomac.2023.123213.
[33] C. Su, J. Liu, Z. Yang, L. Jiang, X. Liu, W. Shao, UV-mediated synthesis of carboxymethyl cellulose/poly-N-isopropylacrylamide composite hydrogels with triple stimuli-responsive swelling performances, Int. J. Biol. Macromol. 161 (2020) 1140–1148, https://doi.org/10.1016/j.ijbiomac.2020.06.094.
[34] L. Wang, Q. Yang, Y. Yang, K. Luo, R. Bai, Porous polyurethane hydrogels incorporated with CMC for eliminating methylene blue from water, Int. J. Smart Nano Mater. 14 (2023) 57–76, https://doi.org/10.1080/19475411.2022.2158958.
[35] J.-Y. Shin, D.Y. Lee, J.I. Yoon, Y.-S. Song, Effect of CMC Concentration on Cell Growth Behavior of PVA/CMC Hydrogel, Macromol. Res. 28 (2020) 813–819, https://doi.org/10.1007/s13233-020-8106-0.
[36] Y.-R. Chen, Z.-X. Zhou, J.-Y. Zhang, F.-Z. Yuan, B.-B. Xu, J. Guan, C. Han, D. Jiang, Y.-Y. Yang, J.-K. Yu, Low-molecular-weight heparin-functionalized chitosan-chondroitin sulfate hydrogels for controlled release of TGF-β3 and in vitro neocartilage formation, Front. Chem. 7 (2019) 745, https://doi.org/10.3389/fchem.2019.00745.
[37] N.S.V. Capanema, A.A.P. Mansur, A.C. De Jesus, S.M. Carvalho, L.C. De Oliveira, H. S. Mansur, Superabsorbent crosslinked carboxymethyl cellulose-PEG hydrogels for potential wound dressing applications, Int. J. Biol. Macromol. 106 (2018) 1218–1234, https://doi.org/10.1016/j.ijbiomac.2017.08.124.
[38] N.F. Alharby, R.S. Almutairi, N.A. Mohamed, Adsorption behavior of methylene blue dye by novel crosslinked O-CM-chitosan hydrogel in aqueous solution: kinetics, isotherm and thermodynamics, Polymers 13 (2021) 3659, https://doi.org/10.3390/polym13213659.
[39] R.C. Gonçalves, R. Signini, L.M. Rosa, Y.S.P. Dias, M.C. Vinaud, R.D.S. Lino Junior, Carboxymethyl chitosan hydrogel formulations enhance the healing process in experimental partial-thickness (second-degree) burn wound healing, Acta Cir. Bras. 36 (2021) e360303, https://doi.org/10.1590/acb360303.
[40] K. Chen, C. Tong, P. JingeYang, Y. Cong, X. Liu, X. Shi, J. Liu, R. Zhang, K. Zou, Y. Xiao, L. Ni, M. Xu, H. Hou, Y. Jin, Liu, Injectable melatonin-loaded carboxymethyl chitosan (CMCS)-based hydrogel accelerates wound healing by reducing inflammation and promoting angiogenesis and collagen deposition, J. Mater. Sci. Technol. 63 (2021) 236–245, https://doi.org/10.1016/j.jmst.2020.06.001.
[41] J. Yang, Y. Chen, L. Zhao, Z. Feng, K. Peng, A. Wei, Y. Wang, Z. Tong, B. Cheng, Preparation of a chitosan/carboxymethyl chitosan/AgNPs polyelectrolyte composite physical hydrogel with self-healing ability, antibacterial properties, and good biosafety simultaneously, and its application as a wound dressing, Compos. Part B: Eng. 197 (2020) 108139, https://doi.org/10.1016/j.compositesb.2020.108139.
[42] T. Zhou, H. Zhou, F. Wang, P. Zhang, J. Shang, L. Shi, An injectable carboxymethyl chitosan hydrogel scaffold formed via coordination bond for antibacterial and osteogenesis in osteomyelitis, Carbohydr. Polym. 324 (2024) 121466, https://doi.org/10.1016/j.carbpol.2023.121466.
[43] R. Aston, K. Sewell, T. Klein, G. Lawrie, L. Grøndahl, Evaluation of the impact of freezing preparation techniques on the characterisation of alginate hydrogels by cryo-SEM, Eur. Polym. J. 82 (2016) 1–15, https://doi.org/10.1016/j.eurpolymj.2016.06.025.
[44] J. Grenier, H. Duval, P. Lv, F. Barou, C. Le Guilcher, R. Aid, B. David, D. Letourneur, Interplay between crosslinking and ice nucleation controls the porous structure of freeze-dried hydrogel scaffolds, Biomater. Adv. 139 (2022) 212973, https://doi.org/10.1016/j.bioadv.2022.212973.
[45] T.-C. Ho, C.-C. Chang, H.-P. Chan, T.-W. Chung, C.-W. Shu, K.-P. Chuang, T.-H. Duh, M.-H. Yang, Y.-C. Tyan, Hydrogels: properties and applications in biomedicine, Molecules 27 (2022) 2902, https://doi.org/10.3390/molecules27092902.
[46] N.F.A.-Z. Tuan Mohamood, A.H. Abdul Halim, N. Zainuddin, Carboxymethyl cellulose hydrogel from biomass waste of oil palm empty fruit bunch using calcium

chloride as crosslinking agent, Polymers 13 (2021) 4056, https://doi.org/10.3390/polym13234056.
[47] M. Khalid, C.T. Ratnam, C.A. Luqman, A. Salmiaton, T.S.Y. Choong, H. Jalaludin, Thermal and dynamic mechanical behavior of cellulose- and oil palm empty fruit bunch (OPEFB)-filled polypropylene biocomposites, Polym. -Plast. Technol. Eng. 48 (2009) 1244–1251, https://doi.org/10.1080/03602550903282986.
[48] E. Akar, A. Altınışık, Y. Seki, Preparation of pH- and ionic-strength responsive biodegradable fumaric acid crosslinked carboxymethyl cellulose, Carbohydr. Polym. 90 (2012) 1634–1641, https://doi.org/10.1016/j.carbpol.2012.07.043.
[49] M. Azizullah, A. Al-Rashida, U. Haider, S.A. Kortz, J.Iqbal Joshi, Development and in vitro anticancer evaluation of self-assembled supramolecular ph responsive hydrogels of carboxymethyl chitosan and polyoxometalate, ChemistrySelect 3 (2018) 1472–1479, https://doi.org/10.1002/slct.201702253.
[50] S. Cai, C. Wu, W. Yang, W. Liang, H. Yu, L. Liu, Recent advance in surface modification for regulating cell adhesion and behaviors, Nanotechnol. Rev. 9 (2020) 971–989, https://doi.org/10.1515/ntrev-2020-0076.
[51] A. Mgharbel, C. Migdal, N. Bouchonville, P. Dupenloup, D. Fuard, E. Lopez-Soler, C. Tomba, M. Courçon, D. Gulino-Debrac, H. Delanoë-Ayari, A. Nicolas, Cells on hydrogels with micron-scaled stiffness patterns demonstrate local stiffness sensing, Nanomaterials 12 (2022) 648, https://doi.org/10.3390/nano12040648.
[52] M. Pan, T. Shui, Z. Zhao, L. Xiang, B. Yan, N. Gu, H. Zeng, Engineered janus hydrogels: biomimetic surface engineering and biomedical applications, Natl. Sci. Rev. (2024) nwae316, https://doi.org/10.1093/nsr/nwae316.
[53] S.H. Arabi, B. Aghelnejad, C. Schwieger, A. Meister, A. Kerth, D. Hinderberger, Serum albumin hydrogels in broad pH and temperature ranges: characterization of their self-assembled structures and nanoscopic and macroscopic properties, Biomater. Sci. 6 (2018) 478–492, https://doi.org/10.1039/C7BM00820A.
[54] R. Panahi, M. Baghban-Salehi, Protein-Based Hydrogels, in: Md.I.H. Mondal (Ed.), Cellulose-Based Superabsorbent Hydrogels, Springer International Publishing, Cham, 2018, pp. 1–40, https://doi.org/10.1007/978-3-319-76573-0_52-1.
[55] Y. Yamada, G. Fichman, J.P. Schneider, Serum protein adsorption modulates the toxicity of highly positively charged hydrogel surfaces, ACS Appl. Mater. Interfaces 13 (2021) 8006–8014, https://doi.org/10.1021/acsami.0c21596.
[56] V. Van Tran, D. Park, Y.-C. Lee, Hydrogel applications for adsorption of contaminants in water and wastewater treatment, Environ. Sci. Pollut. Res 25 (2018) 24569–24599, https://doi.org/10.1007/s11356-018-2605-y.
[57] E. González-Díaz, S. Varghese, Hydrogels as Extracellular Matrix Analogs, Gels 2 (2016) 20, https://doi.org/10.3390/gels2030020.
[58] F. Sharifi, M. Hasani, S.M. Atyabi, B. Yu, B. Ghalandari, D. Li, F. Ghorbani, S. Irani, M. Gholami, Mesenchymal stem cells encapsulation in chitosan and carboxymethyl chitosan hydrogels to enhance osteo-differentiation, Mol. Biol. Rep. 49 (2022) 12063–12075, https://doi.org/10.1007/s11033-022-08013-9.
[59] M.F.M. Gonçalves, A.C. Esteves, A. Alves, Marine fungi: opportunities and challenges, Encyclopedia 2 (2022) 559–577, https://doi.org/10.3390/encyclopedia2010037.
[60] K. Tarman, Marine Fungi as a Source of Natural Products, in: S. Kim (Ed.), Encyclopedia of Marine Biotechnology, 1st ed., Wiley, 2020, pp. 2147–2160, https://doi.org/10.1002/9781119143802.ch96.
[61] L.-E. Petersen, M.Y. Kellermann, P.J. Schupp, Secondary Metabolites of Marine Microbes: From Natural Products Chemistry to Chemical Ecology, in: S. Jungblut, V. Liebich, M. Bode-Dalby (Eds.), YOUMARES 9 - The Oceans: Our Research, Our Future, Springer International Publishing, Cham, 2020, pp. 159–180, https://doi.org/10.1007/978-3-030-20389-4_8.
[62] J.T. Wibowo, A. Bayu, W.D. Aryati, C. Fernandes, A. Yanuar, A. Kijjoa, M.Y. Putra, Secondary metabolites from marine-derived bacteria with antibiotic and antibiofilm activities against drug-resistant pathogens, Mar. Drugs 21 (2023) 50, https://doi.org/10.3390/md21010050.
[63] A.R. Egorov, A.A. Kirichuk, V.V. Rubanik, V.V. Rubanik, A.G. Tskhovrebov, A. S. Kritchenkov, Chitosan and its derivatives: preparation and antibacterial properties, Materials 16 (2023) 6076, https://doi.org/10.3390/ma16186076.
[64] B. Farasati Far, M.R. Naimi-Jamal, M. Jahanbakhshi, A. Hadizadeh, S. Dehghan, S. Hadizadeh, Enhanced antibacterial activity of porous chitosan-based hydrogels crosslinked with gelatin and metal ions, Sci. Rep. 14 (2024) 7505, https://doi.org/10.1038/s41598-024-58174-9.
[65] W. Kruczkowska, K.K. Kłosiński, K.H. Grabowska, J. Gałęziewska, P. Gromek, M. Kciuk, Ż. Kałuzińska-Kołat, D. Kołat, R.A. Wach, Medical applications and cellular mechanisms of action of carboxymethyl chitosan hydrogels, Molecules 29 (2024) 4360, https://doi.org/10.3390/molecules29184360.
[66] Y. Li, Y. Qiu, H. Hou, G. Zhang, H. Hao, J. Bi, The Preparation and properties of amino-carboxymethyl chitosan-based antibacterial hydrogel loaded with ε-polylysine, Foods 12 (2023) 3807, https://doi.org/10.3390/foods12203807.
[67] S. Guan, Y. Wang, F. Xie, S. Wang, W. Xu, J. Xu, C. Sun, Carboxymethyl chitosan and gelatin hydrogel scaffolds incorporated with conductive PEDOT nanoparticles for improved neural stem cell proliferation and neuronal differentiation, Molecules 27 (2022) 8326, https://doi.org/10.3390/molecules27238326.
[68] Y. Yue, Y. Liu, Y. Lin, F. Guo, K. Cai, S. Chen, W. Zhang, S. Tang, A carboxymethyl chitosan/oxidized hyaluronic acid composite hydrogel dressing loading with stem cell exosome for chronic inflammation wounds healing, Int. J. Biol. Macromol. 257 (2024) 128534, https://doi.org/10.1016/j.ijbiomac.2023.128534.
[69] J. Huang, H. Fu, Z. Wang, Q. Meng, S. Liu, H. Wang, X. Zheng, J. Dai, Z. Zhang, BMSCs-laden gelatin/sodium alginate/carboxymethyl chitosan hydrogel for 3D bioprinting, RSC Adv. 6 (2016) 108423–108430, https://doi.org/10.1039/C6RA24231F.
[70] N. KhaliliJafarabad, A. Behnamghader, M.T. Khorasani, M. Mozafari, Platelet-rich plasma-hyaluronic acid/chondrotin sulfate/carboxymethyl chitosan hydrogel for cartilage regeneration, Biotech. Appl. Biochem 69 (2022) 534–547, https://doi.org/10.1002/bab.2130.
[71] Q. Wu, Y. Guo, H. Li, D. Zhang, S. Wang, J. Hou, N. Cheng, M. Huang, L. Luo, Y. Li, Y. Zhao, H. Tan, C. Jin, Recombinant human collagen I/carboxymethyl chitosan hydrogel loaded with long-term released hUCMSCs derived exosomes promotes skin wound repair, Int. J. Biol. Macromol. 265 (2024) 130843, https://doi.org/10.1016/j.ijbiomac.2024.130843.
[72] Q. Garrett, P.A. Simmons, S. Xu, J. Vehige, Z. Zhao, K. Ehrmann, M. Willcox, Carboxymethylcellulose binds to human corneal epithelial cells and is a modulator of corneal epithelial wound healing, Invest. Ophthalmol. Vis. Sci. 48 (2007) 1559, https://doi.org/10.1167/iovs.06-0848.
[73] X. Wang, S. Li, H. Yu, J. Lv, M. Fan, X. Wang, X. Wang, Y. Liang, L. Mao, Z. Zhao, The biocompatibility of multi-source stem cells and gelatin-carboxymethyl chitosan-sodium alginate hybrid biomaterials, Tissue Eng. Regen. Med 19 (2022) 491–503, https://doi.org/10.1007/s13770-021-00429-x.
[74] J. He, F. Wu, D. Wang, R. Yao, Y. Wu, F. Wu, Modulation of cationicity of chitosan for tuning mesenchymal stem cell adhesion, proliferation, and differentiation, Biointerphases 10 (2015) 04A304, https://doi.org/10.1116/1.4932379.
[75] C.M. Murphy, F.J. O'Brien, Understanding the effect of mean pore size on cell activity in collagen-glycosaminoglycan scaffolds, Cell Adhes. Migr. 4 (2010) 377–381, https://doi.org/10.4161/cam.4.3.11747.
[76] F.J. O'Brien, B.A. Harley, M.A. Waller, I.V. Yannas, L.J. Gibson, P.J. Prendergast, The effect of pore size on permeability and cell attachment in collagen scaffolds for tissue engineering, Technol. Health Care 15 (2007) 3–17.
[77] F.J. O'Brien, B.A. Harley, I.V. Yannas, L.J. Gibson, The effect of pore size on cell adhesion in collagen-GAG scaffolds, Biomaterials 26 (2005) 433–441, https://doi.org/10.1016/j.biomaterials.2004.02.052.
[78] X. Wu, H. Li, Incorporation of bioglass improved the mechanical stability and bioactivity of alginate/carboxymethyl chitosan hydrogel wound dressing, ACS Appl. Bio Mater. 4 (2021) 1677–1692, https://doi.org/10.1021/acsabm.0c01477.
[79] Y. Lin, S. Chen, Y. Liu, F. Guo, Q. Miao, H. Huang, A composite hydrogel scaffold based on collagen and carboxymethyl chitosan for cartilage regeneration through one-step chemical crosslinking, Int. J. Biol. Macromol. 226 (2023) 706–715, https://doi.org/10.1016/j.ijbiomac.2022.12.083.
[80] Y. Wang, W. Peng, X. Liu, M. Zhu, T. Sun, Q. Peng, Y. Zeng, B. Feng, W. Zhi, J. Weng, J. Wang, Study of bilineage differentiation of human-bone-marrow-derived mesenchymal stem cells in oxidized sodium alginate/N-succinyl chitosan hydrogels and synergistic effects of RGD modification and low-intensity pulsed ultrasound, Acta Biomater. 10 (2014) 2518–2528, https://doi.org/10.1016/j.actbio.2013.12.052.
[81] W. Xu, Z. Wang, Y. Liu, L. Wang, Z. Jiang, T. Li, W. Zhang, Y. Liang, Carboxymethyl chitosan/gelatin/hyaluronic acid blended-membranes as epithelia transplanting scaffold for corneal wound healing, Carbohydr. Polym. 192 (2018) 240–250, https://doi.org/10.1016/j.carbpol.2018.03.033.
[82] T. Shi, Y. Chen, L. Zhou, D. Wu, Z. Chen, Z. Wang, L. Sun, J. Lin, W. Liu, Carboxymethyl cellulose/quaternized chitosan hydrogel loaded with polydopamine nanoparticles promotes spinal cord injury recovery by anti-ferroptosis and M1/M2 polarization modulation, Int. J. Biol. Macromol. 275 (2024) 133484, https://doi.org/10.1016/j.ijbiomac.2024.133484.
[83] Z. Shi, F. Yang, Q. Pang, Y. Hu, H. Wu, X. Yu, X. Chen, L. Shi, B. Wen, R. Xu, R. Hou, D. Liu, Q. Pang, Y. Zhu, The osteogenesis and the biologic mechanism of thermo-responsive injectable hydrogel containing carboxymethyl chitosan/sodium alginate nanoparticles towards promoting osteal wound healing, Int. J. Biol. Macromol. 224 (2023) 533–543, https://doi.org/10.1016/j.ijbiomac.2022.10.142.
[84] N. Peyravian, P.B. Milan, M.M. Kebria, S. Mashayekhan, M. Ghasemian, S. Amiri, M. Hamidi, A. Shavandi, M. Moghtadaei, Designing and synthesis of injectable hydrogel based on carboxymethyl cellulose/carboxymethyl chitosan containing QK peptide for femoral head osteonecrosis healing, Int. J. Biol. Macromol. 270 (2024) 132127, https://doi.org/10.1016/j.ijbiomac.2024.132127.
[85] C. Gong, J. Yang, D. Zheng, B. Zhou, X. Zhang, X. Wang, X. Huang, Q. Ye, W. Guo, Formulation of O-carboxymethyl chitosan with magnesium phosphate cement promotes in vitro/in vivo angiogenesis and osteogenesis related to the TRPM7 channel in bone regeneration, Compos. Part B: Eng. 280 (2024) 111451, https://doi.org/10.1016/j.compositesb.2024.111451.
[86] S. Arab-Ahmadi, S. Irani, H. Bakhshi, F. Atyabi, B. Ghalandari, Immobilization of cobalt-loaded laponite/carboxymethyl chitosan on polycaprolactone nanofiber for improving osteogenesis and angiogenesis activities, Polym. Adv. Techs 32 (2021) 4362–4372, https://doi.org/10.1002/pat.5438.
[87] X. Zhao, L. Zhou, Q. Li, Q. Zou, C. Du, Biomimetic mineralization of carboxymethyl chitosan nanofibers with improved osteogenic activity in vitro and in vivo, Carbohydr. Polym. 195 (2018) 225–234, https://doi.org/10.1016/j.carbpol.2018.04.090.
[88] L.S.Y. Nanduri, Chitosan–Stem Cell Interactions, in: R. Jayakumar, M. Prabaharan (Eds.), Chitosan for Biomaterials III, Springer International Publishing, Cham, 2021, pp. 343–359, https://doi.org/10.1007/12_2021_83.